

# U-Net and its variants for medical image segmentation: theory and applications

Nahian Siddique <sup>1</sup>, Paheding Sidike <sup>2</sup>, Colin Elkin <sup>1</sup> and Vijay Devabhaktuni <sup>1</sup>

<sup>1</sup> Department of Electrical and Computer Engineering, Purdue University Northwest

<sup>2</sup> Department of Applied Computing, Michigan Technological University

**Abstract:** U-net is an image segmentation technique developed primarily for medical image analysis that can precisely segment images using a scarce amount of training data. These traits provide U-net with a very high utility within the medical imaging community and have resulted in extensive adoption of U-net as the primary tool for segmentation tasks in medical imaging. The success of U-net is evident in its widespread use in all major image modalities from CT scans and MRI to X-rays and microscopy. Furthermore, while U-net is largely a segmentation tool, there have been instances of the use of U-net in other applications. As U-net's potential is still increasing, in this review we look at the various developments that have been made in the U-net architecture and provide observations on recent trends. We examine the various innovations that have been made in deep learning and discuss how these tools facilitate U-net. Furthermore, we look at image modalities and application areas where U-net has been applied.

**Keywords:** U-net; deep learning; medical imaging; segmentation; COVID-19

---

## 1. Introduction

Thanks to recent advances in deep learning in computer vision within the last decade, deep learning has been increasingly utilized in the analysis of medical images. Whilst the use of deep learning in computer vision has seen rapid growth in many different fields, it still faced some challenges in the medical imaging field. There have been many breakthrough techniques over the years to overcome these various challenges. Many techniques and methods have been improvised to developed to such challenges. One such technique that will be discussed in this review will be the U-net, a deep learning technique widely adopted within the medical imaging community.

U-net is a neural network architecture designed primarily for image segmentation [1]. The basic structure of a U-net architecture consists of two paths. The first path is the contracting path, also known as the encoder or the analysis path, which is similar to a regular convolution network and provides classification information. The second is an expansion path, also known as the decoder or the synthesis path, consisting of up-convolutions and concatenations with features from the contracting path. This expansion allows the network to learn localized classification information. Additionally, the expansion path also increases the resolution of the output which can then be pass onto a final convolutional layer to create a fully segmented image. The resulting network is almost symmetrical, giving it a u-like shape. The main canonical task performed by most convolutional networks is to classify the whole image into a single label. However, classification networks fail to provide pixel-level context information which is much needed in medical image analysis. While there have been previous attempts at segmentation tasks, it wasn't until U-net by Ronneberger et al.[1] that there was a significant improvement in medical image segmentation performance. The U-net network was developed based on the works of Long, J et al. [2] using fully convolutional networks. Their implementation achieved better performance than the previous best on the ISBI 2012 challenge and won the ISBI cell tracking challenge in 2015, beating the state of the ray at the time with a considerable margin.

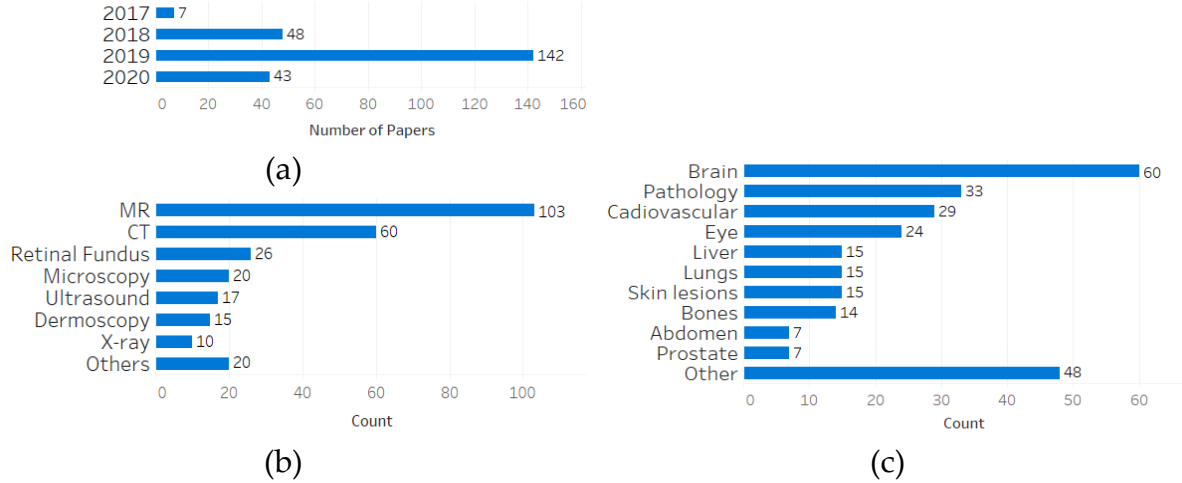


**Figure 1.** (a) Distribution of U-net related papers in our survey by year of publication starting with 2017. (b) Distribution of image modality in U-net related papers. (c) Distribution of application area in U-net related papers. It should be noted that the statistic for 2020 is only till 04/01/2020. We expect the total volume of U-net related papers to be published in 2020 to be proportionally higher than the first three months. It should also be noted that some papers had multiple image modalities and application areas, and each instance was counted separately.

What makes U-net particularly useful is its creation of highly detailed segmentation maps using very limited training samples. The latter trait is of great importance in the medical imaging community as properly labeled images are often limited. This is achieved by utilizing random elastic deformation on the training data which enables the network to learn these variations without requiring new labeled data [1]. Another challenge is to separate touching objects of the same class, which is resolved by applying a weighted loss function that penalizes the model if it fails to separate the two objects. Finally, U-net is also much faster to train than most other segmentation models due to its context-based learning.

Since its inception in 2015, U-net has seen an explosion in usage in medical imaging. And naturally, there have been many advancements in U-net architecture by researchers implementing new methods or incorporating other imaging methods to U-net. In this survey, we go through papers that make use of U-net implementations relating to medical image analysis. To avoid redundancy, only papers since 2017 were reviewed. As there are numerous sources of scientific publicization, in order to find the relevant quality of research papers, we limited ourselves to three major publishers, IEEE, Springer, and Elsevier, and searched their databases with related keywords to find the top papers in each database and collected the appropriate papers. Since new papers are being published regularly, a designated endpoint of 04/01/2020 was selected which was the most recent paper collected in our initial search.

## 2. U-net architectures

### 2.1 Base U-net

As mentioned earlier, the U-net network can be divided into two parts: The first part is the contracting path which uses a typical CNN architecture. Each block in the contracting path consists of two successive 3x3 convolutions followed by a ReLU activation unit and a max-pooling layer. This arrangement is repeated several times. The novelty of u-net comes in the expansive path where at each stage the feature map is upsampled using 2x2 up-convolution. Then, the feature map from the corresponding layer in the contracting path is cropped and concatenated onto the upsampled feature map. This is followed by two successive 3x3 convolutions and ReLU activation. At the final stage, an additional 1x1 convolution is applied to reduce the feature map to the required number of channels and produce the segmented image. The cropping is necessary since pixel features in the edges have the

least amount of contextual information and therefore need to be discarded. This results in a network resembling a u-shape and more importantly, propagates contextual information along the network which allows it to segment objects in an area using context from a larger overlapping area.

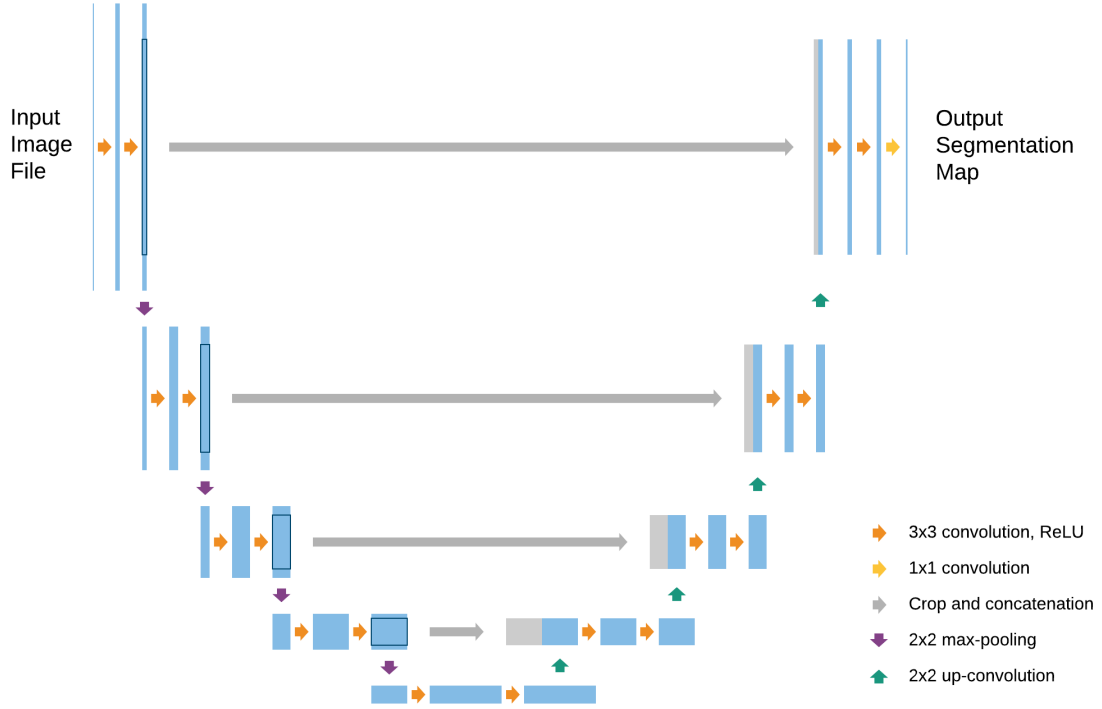


**Figure 2.** Basic U-net architecture. The arrows represent the different operations, the blue boxes represent the feature map at each layer, and the gray boxes represent the cropped feature maps from the contracting path.

The energy function for the network is given by the following equation:

$$E = \sum w(x) \log(p_k(x)), \quad (1)$$

Where  $p_k$  is the pixel-wise SoftMax function applied over the final feature map.

$$p_k(x) = \frac{e^{a_k(x)}}{\sum_{k'=1}^K e^{a_{k'}(x)}} \quad (2)$$

And  $a_k(x)$  denotes the activation in channel  $k$ .

## 2.2 3D U-net

3D U-net is an augmentation of the basic U-net framework that enables 3D volumetric segmentation [3]. The core structure is the same having both a contracting and expansive path. However, all of the 2D operations are replaced with corresponding 3D operations, namely 3D convolutions, 3D max pooling, and 3D up-convolutions resulting in a 3-dimensional segmented image. This network is able to segment images using very few annotated examples. This is due to the fact that 3D images have lots of repeating structures and shapes, enabling a faster training process even with scarcely labeled data. 3D U-net has seen extensive use in volumetric CT and MR image segmentation applications, including diagnosis of the cardiac structures [4]–[11], bone structures [12]–[15], vertebral column [16], [17], brain tumors [18]–[20], liver tumors [21]–[23], lung nodules [24], nasopharyngeal cancer [25], multi-organ segmentation [26]–[28], head and neck organ at risk assessment [29], and white matter tracts segmentation [30]. 3D U-net has been used to great effect in

many biomedical applications. Zeng et al. [12] created a network that produced multi-level segmented images allowing greater abstraction when making a diagnosis.

### 2.3 Attention U-net

An often-desirable trait in an image processing network is the ability to focus on specific objects that are of importance while ignoring unnecessary areas. The attention U-net achieves this by making use of the attention gate [31], [32]. An attention gate is a unit which trims features that are not relevant to the ongoing task. Each layer in the expansive path has an attention gate through which the corresponding features from the contracting path must pass through before the features are concatenated with the upsampled features in the expansive path. Repeated uses of the attention gate after each layer improves segmentation performance significantly without adding too much computational complexity to the model.

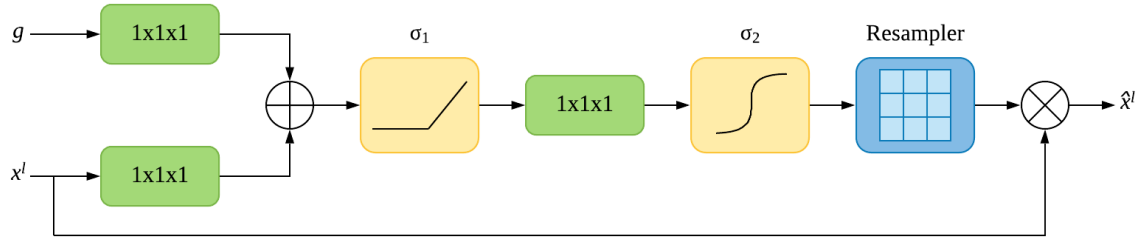


**Figure 3.** Additive attention gate schematic. The input signal  $x^l$  and the gating signal  $g$  both pass through separate  $1 \times 1 \times 1$  convolutions. The signals are then added and undergo a series of linear transformation which are ReLU activation ( $\sigma_1$ ), a  $1 \times 1 \times 1$  convolution, sigmoid activation ( $\sigma_2$ ), and an optional grid resampler. Finally, the original input is concatenated to the output from the sigmoid unit or the resampler.

The attention unit is useful in encoder-decoder models such as the U-net since it can provide localized classification information as opposed to global classification. In U-net this allows different parts of the network to focus on segmenting different objects. Furthermore, with properly labeled training data, the network can attune to particular objects in an image. The attention gate applies a function where the feature map is weighted according to each class and the network can be tuned to focus on a particular class [33], and hence pay attention to particular objects in an image. While there are different types of attention gates, additive attention is more popular in image processing due to it resulting in higher accuracy. The additive attention gate is described by the following:

$$q_{att}^l = \psi^T \left( \sigma_1 (W_{x^l}^T x_i^l + W_g^T g_i + b_g) \right) + b_\psi, \quad (3)$$

$$\alpha_i^l = \sigma_2 (q_{att}^l (x_i^l, g_i; \Theta_{att})) \quad (4)$$

where  $x^l$  is the features from the contracting path and  $g$  is the gating signal. The term  $\sigma_2(x_{i,c})$  represents the sigmoid function:

$$\sigma_2(x_{i,c}) = \frac{1}{1 + \exp(-x_{i,c})} \quad (5)$$

Attention U-net has been applied on problems such as ocular disease diagnosis [34]–[38], melanoma [39], lung cancer [34], cervical cancer [40], abdominal structure segmentation [32], fetus development [32], and brain tissue quantification [41].

### 2.4 Inception U-net

Most image processing algorithms tend to use fixed-size filters for convolutions. Tuning the model to find the correct filter size can often be cumbersome. Moreover, fixed-size filters are

appropriate only for images with similar size salient parts. In many applications, the analysis looks through images with large variations in shapes and sizes in the salient region. One solution to this problem would be to use deeper networks that can read high-level details across a spectrum of sizes and shapes. However, such deep networks are quite computationally expensive. An alternative solution, called the inception network, uses filters of multiple sizes on the same layer in the network. [42]. The outputs from the different filters are concatenated and transferred onto the next layer. The inception network is able to analyze images with different salient regions quite effectively due to the different filter sizes. To reduce computational complexity, the inception network adds a 1x1 convolution before every 3x3 or larger filter for dimensionality reduction. Additionally, pooling layers may also be added parallel in each inception module.



**Figure 4.** (a) The original inception block used in GoogLeNet. (b) Improved inception block with factorized filters. At the end of the inception block, the feature maps from each filter are concatenated together and passed onto the next layer. It should be noted that both networks in figures (a) and (b) are equivalent, though the factorized network requires less computational power.

The original inception network, called GoogLeNet, attained the state of the art outcomes in the ILSVRC14 competition [42]. Soon after, however, more improvements to the network were made. To further improve performance, factorization methods were applied. 5x5 convolution was replaced

with two successive 3x3 convolutions. A single 5x5 convolution is 2.78 times more computationally expensive than two equivalent 3x3 convolutions [43]. Further factorization can be applied by splitting nxn filters into a 1xn and nx1 filter respectively. Factorizing a 3x3 filter by this method makes the network 33% less expensive.

Inception modules of different configurations have been applied on a multitude of U-net applications including brain tumor detection [19], [44], [45], brain tissue mapping [46], cardiac segmentation [7], [47], lung nodule detection [48], human embryo segmentation [49], and ultrasound nerve segmentation [50].

## 2.5 Residual U-Net

This variant of U-net is based on the ResNet [51] architecture. The motivation behind ResNet was to overcome the difficulty in training highly deep neural networks. It is known that neural networks are able to converge faster to a solution the more layers are present. However, experimental results showed that increasing the number of layers results in saturation, and further increases can cause degradation of performance [51]. This degradation arises due to the loss of feature identities in deeper neural networks caused by diminishing gradients in the weight vector. ResNet lessens this problem by utilizing skip connections which take the feature map from one layer and add it to another layer deeper in the network. This behavior allows the network to better preserve feature maps in deeper neural networks and provide improved performance for such deeper networks.

In the residual U-net, at each block in the network, the input to the first convolutional layer is added to the output from the second convolutional layer using a skip connection. This skip connection is applied before the down-sampling or upsampling in the corresponding paths in the U-net. The usage of residual skip connections helps alleviate the vanishing gradient problem [51] allowing for U-net models with deeper neural networks to be designed. Each residual unit can be denoted by the following expressions:

$$y_i = h(x_i) + \mathcal{F}(x_i, \mathcal{W}_i) \quad (6)$$

$$x_{i+1} = f(y_i) \quad (7)$$

Here  $x_i$  and  $x_{i+1}$  correspond to the input and output of the residual unit,  $F(\cdot)$  corresponds to the residual function,  $f(\cdot)$  is the activation function, and  $h(\cdot)$  is the identity mapping function.

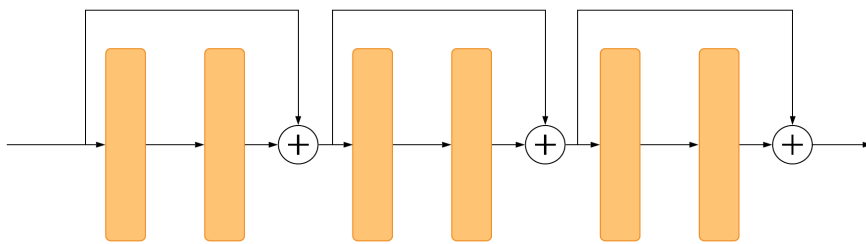


**Figure 5.** Three successive ResNet blocks with skip connections. The skipped signal is joined with the channel output via element-wise addition. The most common ResNet implementations are double layer skips (as shown in this figure) or triple layer skips.

We have found papers where deep residual U-nets have been used to great effect in many biomedical imaging applications such as nuclei segmentation [52], [53], brain tissue quantification [41], brain structure mapping [54], retinal vessel segmentation [55], breast cancer [56], liver cancer [23], [57], prostate cancer [58], endoscopy [59], melanoma [59], osteosarcoma [60], bone structure analysis [61], and cardiac structure analysis [58], [62]. Deep residual U-nets are ideal for complex image analysis.

## 2.6 Recurrent Convolutional Network

Recurrent neural networks are a type of neural network initially designed to analyze sequential data such as text or audio data. The network is designed in such a way so that a node's output is changed based on the previous output from the same nodes; i.e. a feedback loop as opposed to a traditional feedforward network. This feedback loop creates an internal state or memory that provides the node with temporal properties that change the output at discrete time steps. When extended to the entire layer, this allows the network to process contextual information from the preceding data.

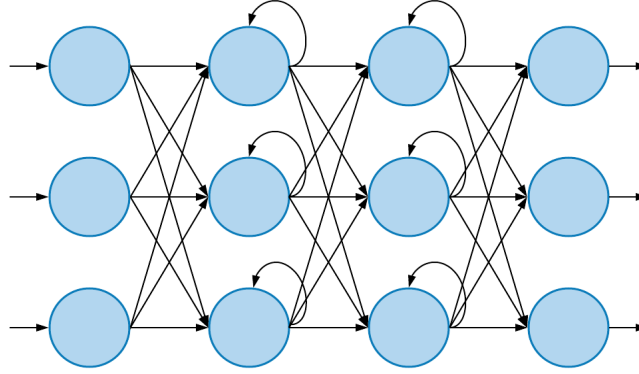


**Figure 6.** Recurrent neural network. In this simple network, the second and third layers are recurrent layers. Each neuron in a recurrent layer receives the feedback from its output as well as new information from the previous layer at discrete time periods and correspondingly produces a new output. This component allows the network to process sequential information.

The recurrent convolutional neural network (RCNN) [63] incorporates the recurrent feedback loops into a convolutional layer. The feedback is applied after both convolution and an activation function and feeds the feature map produced by a filter back into the associated layer. The feedback property allows the units to update their feature maps based on context from adjoining units, providing better accuracy and performance. The output  $y$  of the recurrent convolutional neural network can be expressed as below:

$$y_{ijk}^l(t) = (w_k^f)^T x_i^{f(i,j)}(t) + (w_k^r)^T x_i^{r(i,j)}(t-1) + b_k \quad (8)$$

In this expression  $x(t)$  is the feedforward input and  $x(t-1)$  is the recurrent input for the  $l^{\text{th}}$  layer,  $w^f$  is the feedforward weight,  $w^r$  is the recurrent weight, and  $b$  is the bias of the  $k^{\text{th}}$  feature map. Recurrent convolutional layers have been used in [64], [65]. Alom et al. [52], [66] devised a U-net model containing both recurrent convolution layers and residual connections. The resulting network outperformed solely residual and recurrent U-net models as well as prior state of the art methods using a similar number of parameters.

## 2.7 Dense U-net

Dense U-nets employ DenseNet [67] blocks in place of regular layers. While the ResNet model allows for deeper neural networks, it does not eliminate the problem of vanishing gradients. ResNet architecture also eventually degrade in performance with increasing layers. DenseNet is a deep learning architecture built on top of ResNet with two key changes. Firstly, every layer in a block receives the feature or identity map from all of its preceding layers [67]. And the second major change is that the identity maps are combined via channel-wise concatenation into tensors [67] as opposed to ResNet where the identity maps are summed via element-wise addition. Therefore, the identity mapping of each layer is dependent not only on the previous layer but on all of the layers before it in the block. This allows DenseNet to preserve all identity maps from prior layers and significantly promote gradient propagation. The implication is that each layer can have fewer

channels as information is more easily preserved between layers resulting in higher accuracy with fewer computations and as a consequence can allow deep learning models with a greater number of layers. The output for each layer in a dense block is described below:

$$x_i = H_i([x_0, x_1, x_2, \dots, x_{i-1}]) \quad (9)$$

Where  $H_i(\cdot)$  represents the dense mapping function which usually includes batch normalization, ReLU activation, and a convolutional layer while  $[]$  denotes channel-wise concatenation.

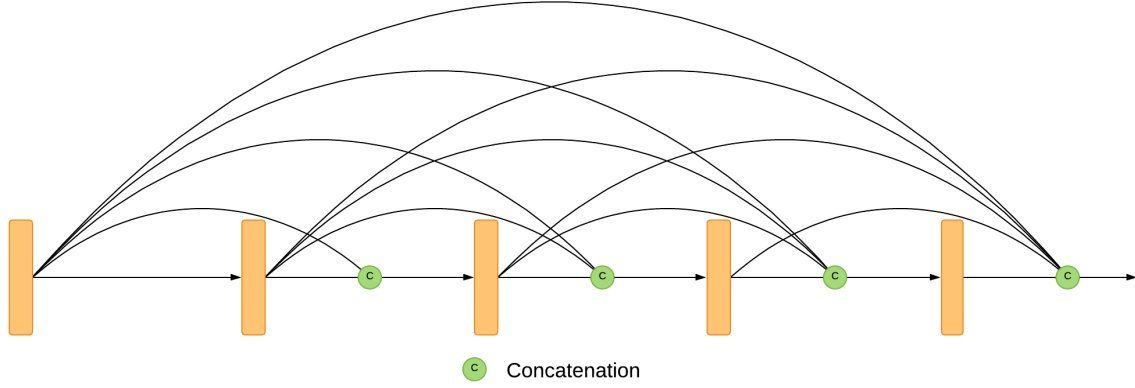


**Figure 7.** A five-layer dense block. The concatenation unit receives the feature map from all previous layers and passes it onto the next layer. This ensures that any given layer has contextual information from any of the previous layers in the block.

When implementing a U-net, each traditional U-net block is replaced with a dense block of two or more convolutional layers. The adoption of dense blocks allows for deeper U-net models which can segment objects in an image with greater distinction. This attribute of dense U-nets is highly sought after in medical image analysis due to objects in such images being extremely close and often overlapping. Applications of dense U-net have been found in analysis of brain tumors [20], [45], retinal blood vessel segmentation [45], cerebral blood vessel segmentation [68], [69], melanoma [70], lung cancer [70], liver cancer [71], and multi-organ segmentation [72].

### 2.8 U-net++

U-net++ is another powerful form of the U-net architecture inspired from DenseNet [67]. It uses a dense network of skip connections as an intermediary grid between the contracting and expansive paths [73]. This aids the network by propagating more semantic information between the two paths enabling it to segment images more accurately.

In traditional U-net, the feature maps of the contracting path are directly concatenated onto the corresponding layers in the expansive path. U-net++ however has a number of skip connection nodes between each corresponding layer. Each skip connection unit receives all of the feature maps from all previous units at the same level as well an upsampled feature map from its immediate lower unit. Therefore, each level is equivalent to a dense block. This arrangement minimizes the loss of semantic information between the two paths. The operation of the skip connection unit is as follows, where  $x$  represents the feature map and  $i$  and  $j$  correspond to the index down the contracting path and across the skip connections respectively:

$$x^{ij} = \begin{cases} \mathcal{H}(x^{i-1j}), & j = 0 \\ \mathcal{H}([x^{ik}]_{k=0}^{j-1}, U(x^{i+1j-1})), & j > 0 \end{cases} \quad (10)$$

Here  $H(\cdot)$  denotes a convolution and activation operation,  $U(\cdot)$  represents the up-sampling operation, and  $[]$  signifies a concatenation. The number of intermediary skip connection units depends on the layer number and decreases linearly going down the contracting path. Applications

in U-net++ include segmentation of cell nuclei [73], cancer tissue [73], cardiac structures and vessels [74], [75], and pelvic organs [76].

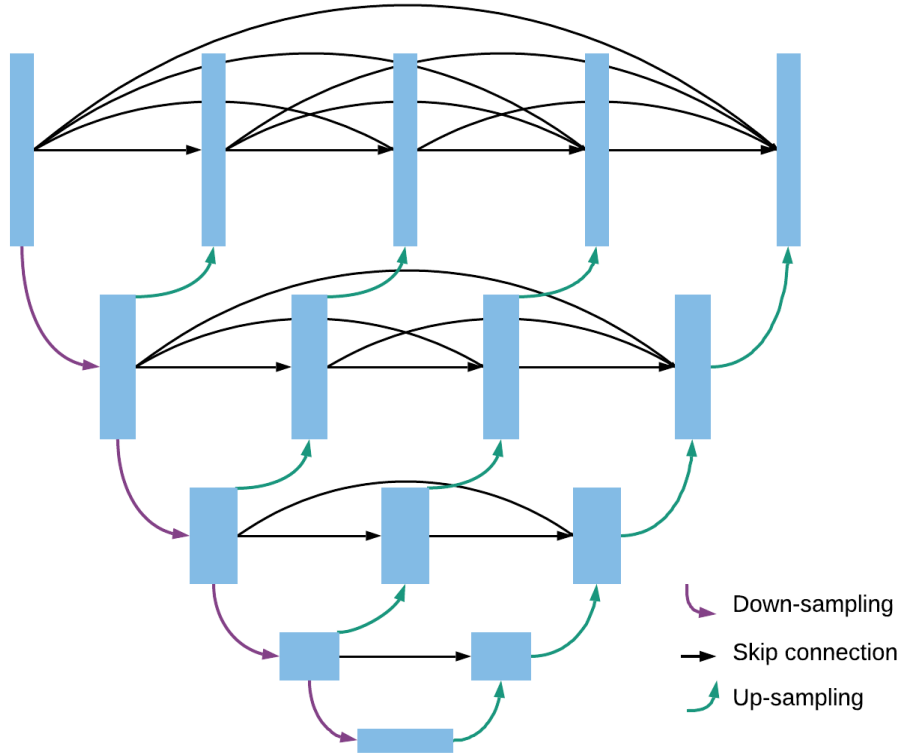


**Figure 8.** U-net++ schematic representation. Each square denotes a convolutional block. Unlike base U-net, which has a single direct concatenation from the contracting path to the expansive path, U-net++ has a series of intermediary convolutional blocks between the two paths. Each intermediary and expansive block receives the concatenated feature maps from all of the previous blocks at the same level as well as the upsampled feature map from the block immediately below it.

### 2.9 Adversarial U-net

An adversarial model is a setup where two networks compete against each other in order to improve their performance. Generative adversarial networks (GAN) are a novel type of adversarial process used to generate new data [77]. The framework consists of two networks: a discriminator and a generator. The discriminator network  $D$ , is a classifier that is trained to identify whether a given input image came from the data set or produced by the generator  $G$ . The discriminator  $D$  undergoes standard CNN supervised training and for each image input, it outputs the probability of the image being produced by  $G$  with the goal of minimizing its error rate of classifying ‘fakes’ as real data set images. The generator  $G$  produces images that are periodically fed to the discriminator. To help the generator produce convincing images, its gradient function is a function of the discriminator’s gradient function during the step the discriminator is fed a fake image. This allows the generator to adjust its weight in response to the output of the discriminator. Furthermore, to create variations in the images produced by the generator, random noise is passed to it. The goal of the generator is to deceive the discriminator, i.e. maximize the error rate of the discriminator. This minimax relationship results in an adversarial network where the two networks compete with each other.

$$\min_G \max_D V(D, G) = \mathbb{E}_{x \sim p_{\text{data}}(x)} \log D(x) + \mathbb{E}_{z \sim p_z(z)} \log(1 - D(G(z))) \quad (11)$$

Given enough time the adversarial network should reach an optimal state where the discriminator always outputs a probability of  $\frac{1}{2}$  regardless of whether the image is from the data set or the generator [77], meaning it can no longer distinguish the real images from the synthetic images produced by the generator. The resulting generator can then be used to artificially create images of a particular subject.

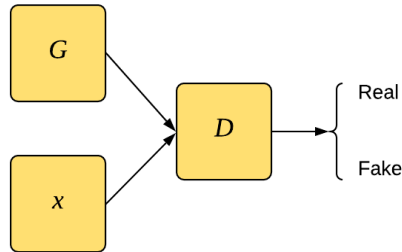


**Figure 9.** GAN block diagram. The goal of network  $D$  is to classify all inputs from  $x$  and network  $G$  as real and fake respectively. The goal of  $G$  is to have its output evaluated as real.

This framework can be further extended to restrict the GAN into producing a limited band of synthetic images by controlling its labels and input images. This alteration is known as a conditional GAN [78]. Adversarial U-nets are a type of conditional GANs. The generator network is constructed based on the U-net architecture while the discriminator remains the same. The U-net design allows the generator to take an image as input instead of random noise. The key difference in adversarial U-nets is that the goal of the generator is not to produce new images, but rather transformed images. This output of the generator  $G$  is evaluated against the discriminator  $D$  which is trained on manually transformed images. Ideally, after proper training, the generator will be able to achieve the same transformation ability as the manual human transformation. The resulting generator can then be used to apply its transformation function on new images which would be considerably faster than a physician manually converting the image. Adversarial U-nets have seen a wide spectrum of applications including quantitative susceptibility mapping of the brain [79], detection of brain tumors [80], [81] and breast cancer [82], segmentation of retinal vessels [38], segmentation of cardiac structures [83], and image registration of brain structures [84].

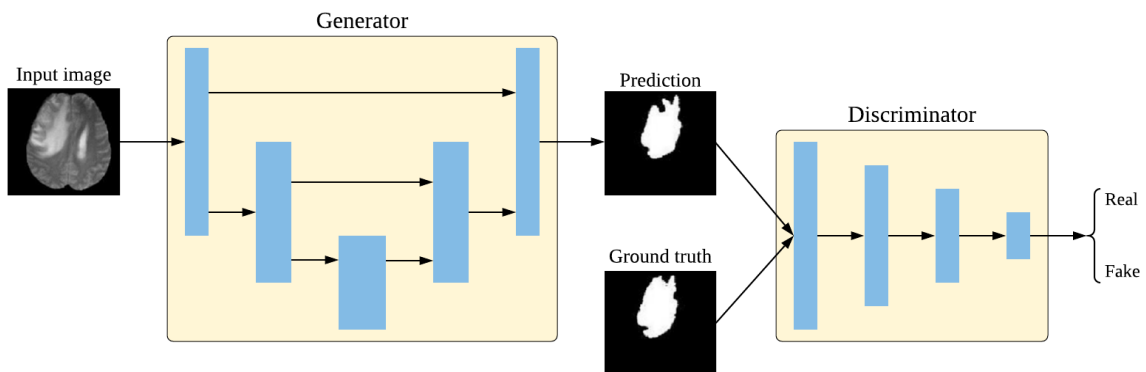


**Figure 10.** Simplified schematic of U-net based GAN. The generator synthesizes predictions for the tumor area from the input images. The predictions are fed into the discriminator which judges the accuracy of the prediction by evaluating its similarity to the ground truth. If the prediction is similar to the ground truth then the discriminator will be unable to distinguish between them and classify the prediction as real. Given enough training, the GAN will be able to segment images to the same accuracy and precision as manual annotations [81].

### 2.10 Cascaded arrangement

In addition to the aforementioned architectures, various other network configurations have also been tested for U-net. One such method is cascading two or more U-nets. In this arrangement, the first layer performs a high-level segmentation, with each successive U-net performing segmentation on smaller objects. Feng et al. [85] designed a two-stage U-net model where the first U-net segments the liver from other organs and the second U-net segments tumors within the liver. Liu et al. [57] designed a two-stage U-net for liver segmentation with an intermediate processing module between the two U-nets. Xu et al. [8] and Li et al. [44] have both designed two-stage cascaded U-nets where the first network is a 2D U-net and the second network is a 3D U-net. Other two-stage U-net models are implemented in [5], [6], [29], [53], [71], [86]–[89]. While two-stage networks are the most common type of cascaded U-nets, we have found two instances of cascaded U-nets with variable numbers of stages [90], [91]. In all of these papers, the cascaded U-net performed better than a single U-net.

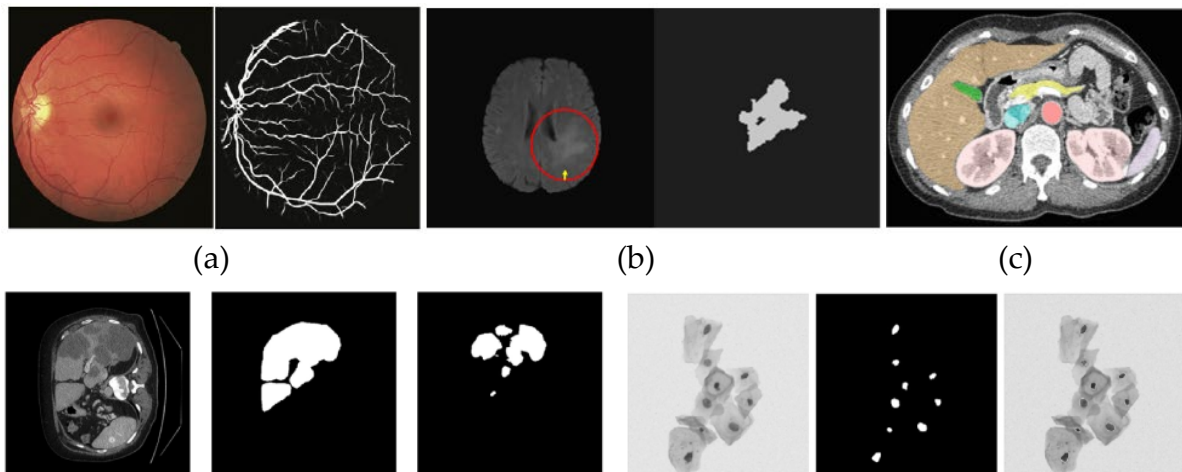
### 2.11 Parallel arrangement

Yet another arrangement of the overall architecture can be found in the form of a parallel arrangement of part or the entirety of a U-net network. Abd-Ellah et al. [92] arranged two parallel U-nets and aggregated the results for improved segmentation accuracy. Soltanpour et al. [93] implemented four parallel U-nets with each segmenting a different CT map and then merging the results. A halfway point can be achieved by parallel encoders, which allow for better extraction of features [94]–[96]. Murugesan et al. [97] implemented a network with parallel decoders that provide different levels of segmentation.

2.5D U-net is a special architecture where three 2D U-net networks are run parallelly on different 2D projections of a 3D image to produce a 3D segmentation map. The 2D U-nets perform slice by slice segmentation on the 3D volume along three different axes, and the final 3D segmentation is computed by fusing the results [98]–[101]. The advantage of the 2.5D parallel arrangement is reduced computational load for segmentation when juxtaposed with an equivalent 3D network.

## 3. Image modalities

Segmentation is the primary task for U-net models. The goal of segmentation tasks is to outline and separate different objects in an image, i.e. to classify different objects rather than classifying the whole image. This is of particular importance in the medical imaging community as the diagnosis of medical conditions requires careful analysis of local regions in an image. For instance, the diagnosis of brain tumors would require separating the tumors from the rest of the brain structures. We have found extensive use of the U-net architecture for an assortment of medical imaging analysis. In the next section, we discuss the major image modalities on which U-net has been applied.



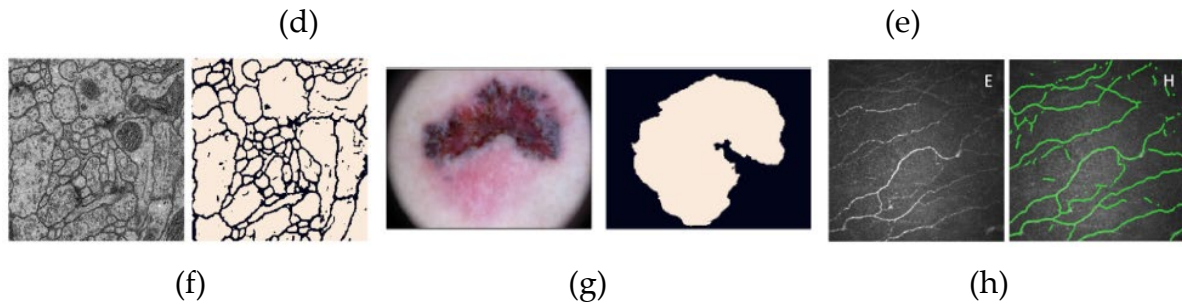


**Figure 11.** Examples of U-net applications. Images have been collected from papers in this survey. (a) Retinal vessel segmentation [102]. (b) Brain tumor detection and segmentation [103]. (c) Multi-organ abdominal segmentation (liver; spleen; left and right kidneys; pancreas; gallbladder; aorta; and inferior vena cava) on CT scans [27]. (d) Liver tumor segmentation, left to right: original CT image, liver segmentation image, and lesion segmentation image [104]. (e) Nuclei prediction, from left to right: original cell images, prediction of nuclei, labeling nuclei in the original images [40]. (f) Cell segmentation [59]. (g) Skin lesion segmentation [59]. (h) Corneal nerve segmentation [105].

### 3.1 Magnetic resonance imaging (MRI)

MRI is a very popular radiology imaging technique used to take pictures of soft tissue inside the body. In our review, we have found MRI to be the most popular image modality for segmentation using U-net. MRI is a useful diagnostic tool particularly for analysis of the brain. U-net has been used extensively in this regard for the segmentation of brain structures. Various U-net models have been applied on MR images for brain tumor diagnosis [18], [19], [59], [45], [81], [106], [107], [87], [108]–[111], [92], [112]–[119], [44], [120]. U-net has also been applied on brain tissue for investigation of neurological conditions [54], [101], [103], [121]–[124], analysis of white matter tissue [125]–[127], [89], fetal brain development [128]–[131], and stroke lesions [69], [132]–[136].

U-net implementation has also been applied on cardiovascular MR images [4]–[6], [8]–[11], [47], [58], [62], [74], [83], [86], [90], [137]–[146] to segment structures of the heart. Cancer is a leading cause of deaths worldwide and MR is one of the strongest methods for proper prognosis of various types of cancers. In addition to brain cancer, we have found applications on prostate cancer [58], [64], [147]–[151], liver cancer [21], [152], [153], nasopharyngeal cancer [25], [98], [154], and breast cancer [99], [155]. Other implementations include segmentation of the femur [12]–[14], spinal cord [156], [157], blood vessels [100], vertebral column [17], human placenta [158], and the uterus [159].

**Table 1.** Applications of U-net based models for MR image analysis.

Reference	Model/Methods used
Brain tumor	
[106], [107], [110]–[112], [114]–[118]	Base U-net
[18], [109], [120]	3D U-net
[81]	Adversarial net; GAN
[59], [108]	Residual block
[113]	Dense block
[87]	Cascaded U-net
[92]	Residual block; Parallel U-net
[44]	Inception block; Up skip connections
[45]	Dense block; Inception block
[119]	3D U-net; Residual block
[19]	3D U-net, Inception block, Residual block
Brain tissue	
[103], [121]–[124]	Base U-net
[28], [160]	3D U-net
[161]	2.5D U-net

[54]	Residual block
[101]	Parallel U-net
[41]	Attention gate; Residual block
White matter tracts	
[126], [127]	U-net with modified skip connections
[125]	Base U-net
[89]	Cascaded U-net
Fetal brain	
[128]–[130]	Base U-net
[131]	Base U-net; 3D U-net
Stroke lesion/thrombus	
[133]–[136]	Base U-net
[132]	3D U-net
[69]	Dense block; Inception block
Cardiovascular structures	
[138], [140]–[142], [144], [146]	Base U-net
[62], [139], [143], [145]	Residual block
[4], [9], [10], [28]	3D U-net
[86], [90]	Cascaded U-net
[5], [8]	Cascaded 3D U-net
[11]	Base U-net; 3D U-net
[83]	Adversarial net; GAN
[58]	Residual block
[137]	Dense block
[74]	U-net++
[47]	Inception block; Residual block
[6]	Cascaded 3D U-net; Residual block
Prostate cancer	
[147], [149]–[151]	Base U-net
[28]	3D U-net
[64]	Recurrent net
[58]	Residual block
Liver cancer	
[152], [153]	Base U-net
[21]	3D U-net
Nasopharyngeal cancer	
[25]	3D U-net; Residual block
[98]	Parallel U-net
[154]	Modified convolution block
Femur	
[12]–[14]	3D U-net
Breast cancer	
[155]	Base U-net
[99]	Parallel U-net
Spinal cord	
[156], [157]	Base U-net
Blood vessels	
[100]	Base U-net
Placenta	
[158]	Base U-net
Uterus	
[159]	Base U-net
Vertebral column	
[17]	3D U-net

### 3.2 Computed tomography (CT)

CT scans are another major non-invasive medical analysis tool for analyzing internal organs and tissue. As with MRI, cancer diagnosis is a major area where CT imaging is applied; liver cancer [22], [23], [57], [71], [73], [85], [94], [104], [162]–[164], lung cancer [24], [34], [45], [48], [70], [73], [165]–[169], bone cancer [60], and cervical cancer [170]. CT scans are also used for multiorgan abdominal segmentation [26], [27], [32], [72], [151], [171]. CT scans have also been used for the segmentation of hard tissue such as bones [14]–[16], [60], [76], [172]. Along with MR imaging, CT is one of the few imaging techniques that can produce 3D images. The versatility of CT imaging makes a favored modality in medical diagnosis.

**Table 2.** Applications of U-net based models for CT image analysis.

Reference	Model/Methods used
Liver cancer	
[104], [162], [163]	Base U-net
[22], [28]	3D U-net
[23]	3D U-net; Residual block
[73]	U-net++
[85]	Cascaded U-net
[57]	Cascaded U-net; Residual block
[71]	Cascaded U-net; Dense block
[94]	Modified U-net with dual parallel encoders
Lung cancer	
[165]–[167]	Base U-net
[168], [169]	Residual block
[34]	Attention gate
[24]	3D U-net; Residual block
[48]	Dense block; Inception block
[73]	U-net++
Pulmonary tissue	
[173], [174]	Base U-net
[175]	Residual block
Abdominal organs	
[151], [171]	Base U-net
[26], [27]	3D U-net
[32]	Attention gate
[72]	Dense block
Cardiovascular structures	
[4]	3D U-net
[86]	Cascaded U-net
[5]	Cascaded 3D U-net
[119]	3D U-net; Residual block
[7]	3D U-net; Inception block
[75]	U-net++
Pancreas	
[156], [176], [177]	Base U-net
[28]	3D U-net
Bones	
[172]	Base U-net
[14]	3D U-net
[15]	3D U-net; Residual block
[60]	Residual block
[76]	U-net++
Stroke lesions	

[93], [178]	Base U-net
[132]	Base U-net; 3D U-net
[69]	Dense block; Inception block
Head and neck	
[179]	3D U-net
[29]	Cascaded 3D U-net
Gallstones	
[180]	U-net++
[88]	Cascaded U-net
Liver and spleen	
[164]	Dense block
Blood vessels	
[181]	Residual block
Brain	
[46]	Inception block; Residual block
[95]	Modified U-net with dual parallel encoders
Cervical cancer	
[170]	Base U-net
Fetus	
[32]	Attention gate
Melanoma	
[70]	Dense block
Vertebral column	
[16]	3D U-net

### 3.3 Retinal fundus imaging

Color fundus imaging is an ophthalmology technique used for the detection and diagnosis of various ocular diseases such as glaucoma, diabetic retinopathy, age-related macular degeneration (AMD), etc. Proper prognosis depends on the precise segmentation of key structures such as retinal blood vessel segmentation [55], [182]. Accurate screening is of chief importance since such diseases often need to be diagnosed early for treatment. Though ophthalmic imaging has a far narrower scope than MR and CT, the retinal fundus is one of the most analyzed structures in our survey right after the brain and cardiovascular system. As it is the primary method of imaging the retina, we expect more research on fundus image analysis to continue as well as research on more complex retinal fundus images.

**Table 3.** Applications of U-net based models for fundus image analysis.

Reference	Model/Methods used
[102], [182]–[190]	Base U-net
[34]–[36], [191]	Attention gate
[55], [169], [192], [193]	Residual block
[70]	Dense block
[38]	Adversarial net; GAN; Attention gate
[91]	Cascaded U-net
[194]	Attention gate; Residual block
[45]	Dense block; Inception block
[195]	Inception block; Residual block
[97]	Modified U-net with parallel decoders
[196]	Recurrent residual block; Up skip connections

### 3.4 Microscopy

Microscopy refers to the examination of extremely small objects that cannot be observed with the naked eye. It should be noted that in our survey we refer to microscopy to mean only optical

microscopy. This modality is used extensively in pathology. One of the major challenges in microscopy imaging is identifying overlapping cells as well as identifying the boundary between cells. These are unique challenges to microscopy as smaller structures such as cells and tissues often don't have well-defined landmarks and similarities that make it harder for image processing. However, U-net has overcome such challenges [1] and continues to be a strong implementation for this modality.

**Table 4.** Applications of U-net based models for microscopy image analysis.

Reference	Model/Methods used
Cell nuclei	
[197]	Base U-net
[59], [198], [199]	Residual U-net
[52]	Recurrent net; Residual block
[53]	Cascaded U-net; Residual block
[73]	U-net++
Cell contour	
[200], [201]	Base U-net
[40]	Attention U-net
Human embryo	
[202]	Base U-net
[49]	Inception block
Corneal nerve	
[105]	Base U-net
[36]	Attention gate
Chromosomes	
[203], [204]	Base U-net
Blood vessels	
[205]	Base U-net
Parasite detection in Chagas disease	
[206]	Base U-net
Sclerosis	
[207]	Base U-net
Colon gland	
[208]	Base U-net

### 3.5 Dermoscopy

Dermoscopy is a detailed examination of the skin. It is almost exclusively used to examine skin diseases such as skin lesions. The primary medical condition diagnosed using Dermoscopy images in our survey is melanoma or skin cancer, though we have found a single paper on psoriasis diagnosis [209]. The performance of Dermoscopy image analysis methods is of keen interest in the medical imaging community since it is often used for early detection of melanoma and is less costly than other noninvasive diagnostic tools.

**Table 5.** Applications of U-net based models for Dermoscopy image analysis.

Reference	Model/Methods used
Melanoma	
[210]–[218]	Base U-net
[39]	Attention gate
[59]	Residual block
[70]	Dense block
[194]	Attention gate; Residual block
[196]	Up skip connections
Psoriasis	

### 3.6 Ultrasound

Medical ultrasound is yet another noninvasive imaging technique for the analysis of internal structures. Ultrasound is mostly used for early and real-time diagnosis. Additionally, unlike many other image modalities, ultrasound devices are more maneuverable and can capture images from multiple angles. Ultrasound is also safe since it does not use radiation, hence it is the primary imaging modality for pregnancy-related diagnosis [219]–[221]. Medical ultrasound use cases also include analysis of soft tissue such as nerve bundles [39], [50], [151], [222], [223]. Its real-time image capture makes it extremely useful in tracking objects [96].

**Table 6.** Applications of U-net based models for ultrasound image analysis.

Reference	Model/Methods used
Nerve segmentation [151], [222]	Base U-net
[50]	Inception block
[223]	Residual block
[224]	Modified parallel U-net
Breast lesion [225]	Base U-net
[39]	Attention gate
Arterial wall [226]	Base U-net
Cardiovascular structures [227]	Base U-net
Fetal head [219]	Base U-net
Gastrointestinal tumor [228]	Base U-net
Knee cartilage [96]	Modified U-net with dual parallel encoders
Preterm birth prediction [220]	Base U-net
Thyroid [229]	Residual block
Transcranial detection [221]	Base U-net
Ovary detection [230]	Base U-net

### 3.7 X-ray

X-ray is a radiograph method used mainly for the imaging of hard tissue. It is the most widely used technique for the analysis of bones. U-net models have been applied to X-rays of bones for diagnosis of rheumatoid arthritis and osteoporosis [61], [231], and other bone-related diseases. Chest x-rays are also fairly prevalent and used for the detection of a myriad of pulmonary diseases including tuberculosis [194]. Aside from that, we have found applications of U-net in the detection of coronary stenosis [232], breast tumors [82], and surgical catheters [233].

**Table 7.** Applications of U-net based models for X-ray image analysis.

Reference	Model/Methods used
Phalange bones [231], [234]	Base U-net

[61]	Residual block
Chest organs	
[235]	Base U-net
[34]	Attention gate
[194]	Attention gate; residual block
Pelvic bones	
[236]	Base U-net
Blood vessel segmentation	
[232]	Base U-net
Breast tumor	
[82]	Adversarial net; GAN
Surgical catheter detection	
[233]	Residual block

### 3.8 Other Modalities

In addition to commonly used image modalities, we have also found u-net applications on more inconspicuous modalities. Endoscopy is an invasive imaging procedure where the imaging device is inserted into an organ or cavity to take pictures. U-net has been applied to endoscopy images for segmentation of polyps in the gastrointestinal tract [97], [237], colon objects [59], and detection of laryngeal leukoplakia [65]. On electron microscopy images, applications were detection of neuronal structures [156], [238], cell contour [156], and viruses [239]. Optical coherence tomography (OCT) is an imaging method for taking cross-sectional images of the retina. OCT is used for the diagnosis of various ocular diseases, for instance, age-related macular degeneration (AMD), retinal vein occlusion, and diabetic macular edema [240]. U-net has been used on OCT for segmentation of retinal layers [241], blood vessels [242], fluid regions [243], and Drusen [244]. Other uncommon applications are segmentation of blood vessels in digital subtraction angiography (DSA) [68], [245], white matter tract segmentation in diffusion tensor imaging [30], iris segmentation in iris imaging [37], and tumor detection in mammograms [56].

**Table 8.** Applications of U-net based models for various image modalities.

Reference	Model/Methods used	Image Modality
[103], [237]	Base U-net	Endoscopy
[59]	Residual block	Endoscopy
[65]	Cascaded U-net; Recurrent residual net	Endoscopy
[97]	Modified U-net with parallel decoders	Endoscopy
[156], [238], [239]	Base U-net	Electron microscopy
[169]	Residual block	Electron microscopy
[240]–[244]	Base U-net	OCT
[245]	Base U-net	DSA
[68]	Dense block	DSA
[30]	3D U-net	DTI
[37]	Attention gate	Iris imaging
[56]	Residual block	Mammogram

## 4. Other Canonical Tasks by U-net

Even though U-net is an algorithm developed for segmentation, it has seen a modest amount of augmentation for other types of tasks. Image analysis is often hampered by the presence of noise or loss of detail during imaging. We have found three papers where U-net was implemented to remove artifacts from images by reconstructing the images [79], [246], [247] as well as a paper where U-net was used for de-aliasing [80]. Image registration is also an area where U-net model has seen experimentation [84], [248], [249]. Other reconstruction tasks include the correction of infant cortical surface [250] and EPID dosimetry correction of the cerebrospinal region [251]. Other outlier usages

include synthesis of medical images [252], image super-resolution [20], and data augmentation to enable easier annotation of medical images [253].

**Table 9.** Applications of U-net based models on other canonical tasks.

Reference	Image modality	Canonical task	Model/Methods	Application area
[246]	CT	Denoising	Modified U-net	Cervix
[247]	Ultrasound	Denoising	Base U-net	Brain tissue
[79]	MR	Denoising	3D adversarial net	Brain tumor
[80]	MR	De-aliasing	Adversarial net	Brain tumor
[248], [249]	MR	Image registration	Base U-net	Brain tissue
[84]	MR	Image registration	Adversarial net	Brain tissue
[250]	MR	Image correction	3D U-net	Brain surface
[251]	EPID dosimetry	Image correction	Base U-net	Brain and spinal cord
[252]	CT; MR	Image synthesis	Base U-net	Brain tissue
[253]	MR	Data augmentation	Base U-net	Brain tissue
[20]	MR	Superresolution	3D U-net; Dense block	Brain tumor

## 5. Discussion

Deep learning techniques such as U-net have seen increasing uses in medical image analysis over the years. Deep learning in image processing has allowed a variety of different tasks such as classification, detection, localization, etc. Segmentation tasks however are of keen interest in the medical imaging community. Surveys carried out by [254], [255] reveal that segmentation is the most sought out canonical task in medical image analysis. This is further evident by the abundance of papers published specifically for segmentation tasks, where U-net and its variants continue to be a prominent method [256]. The examination of U-net in this survey provides some answers to its high utility. In addition to being a well-performing segmentation model, a feature of U-net that makes it incredibly valuable is its high modularity and mutability. We have provided in this review numerous papers that have incorporated other deep learning methods into U-net, including some papers adopting multiple models at once. These alterations change the low-level architecture of the U-net while keeping the high-level design the same. More importantly, this means two things: the first is that this provides U-net a wide spectrum of applications since it can be greatly tuned depending on the application at hand. The second is that this means U-net still has a lot of potential for advancement since its modular nature allows it to keep on improving by incorporating newer novel ideas into itself.

For the specific use cases of the survey, we have found MR to be the most popular image modality though there remains a healthy variety of other image types. The same holds true for application areas, where U-net has been successfully implemented for both popular and niche applications. We would also like to point out to the alternate tasks performed in papers in this survey; although few, these tasks provide U-net with another avenue for exploration.

### 5.1 Challenges

The success of deep learning is vital for improved medical diagnosis. Although there has been tremendous progress in deep learning techniques such as U-net in the past decade, the nature of medical analysis demands algorithms to perform with minimal error. A major limitation of reducing this error in deep learning techniques is computational power. Powerful deep learning algorithms require more time to train and hence are less feasible. U-net algorithms have applied transfer learning as one solution to alleviate this problem [235]. EfficientNet is a framework for optimizing neural network construction that has the potential to streamline U-net design, making it more powerful using a similar number of parameters [257]. Another critical problem is the scarcity of annotated data for training. Ronneberger et al. [1] proposed a solution is his original U-net paper of applying random deformation to create new samples. An alternative solution is the use of adversarial models like GAN to synthesize new image samples. GAN in particular has seen

tremendous success in synthesizing medical images [258]. Finally, deep learning models have the problem of being ‘black boxes’; the input and output to the network are well understood, but the behavior of the internal hidden layers are not. This creates a problem where researchers often do not understand how to fix errors in the network or which layers or filters are more important to the task. Additionally, black boxes are difficult to interpret properly and their properties are difficult to replicate [259]. These are some key reasons why deep learning is yet to be used in any large scale real-world medical trial [260], despite its tremendous promise. However, day by day these problems are becoming easier to overcome and we expect to see even greater adoption of deep learning in the medical imaging community. In this regard, we expect U-net to be a major stepping stone in deep learning within the realm of medical image analysis.

## 5.2 U-net for COVID-19

The novel coronavirus (COVID-19) pandemic has created a staggering global medical crisis. As of June 22nd, a total of 8,708,008 cases and 461,715 deaths have been recorded globally [261]. To combat this challenge, the medical imaging community has involved itself in the research of various deep learning techniques, including U-net, for diagnosis of COVID-19. The primary diagnostic images taken for COVID-19 are chest CT scans which are ideal since U-net has seen extensive exploration in that modality. The versatility of the U-net network has allowed rapid development and deployment of early screening diagnostic algorithms for field use as early as March 2020 [262]. Further improvements on early screening tests have been made by augmenting attention and residual methods with U-net [263], [264]. Wu et al. [265] have implemented a hybrid network with U-net for segmentation and a classifier for classification. Yan et al. [266] developed a network with feature variation that allowed for an easier distinction of COVID-19 infection. U-net research has also been ongoing in X-ray based screening of COVID-19 [267], [268]. Alom et al. [269] established a multi-stage model to detect COVID-19 from X-ray and CT images. A survey on deep learning techniques for COVID-19 diagnosis reveals that U-net is one of the primary models of choice for segmentation related tasks [270]. This is no surprise as we have already explored the various utilities of U-net based models. We expect research on U-net based algorithms for the diagnosis of COVID-19 to continue and be a major asset to the medical imaging community during this global crisis.

## 6. Conclusions

In this survey, we hope to provide a starting point for researchers who wish to explore U-net, a powerful deep learning model used extensively for medical image segmentation. We explore the many variants of U-net and its diverse applications on a multitude of image modalities. We also breakdown the major deep learning methods and their application areas for all of the papers in this survey. It is concluded that U-net based architecture is indeed quite ground-breaking and valuable in medical image analysis. The growth of U-net papers since 2017 lends credence to its status as a premier deep learning technique in medical image diagnosis. Despite the many challenges remaining in deep learning-based image analysis, we expect U-net to be one of the major paths forward.

## 7. Resources

### 7.1 Frameworks

There are many open-source deep learning frameworks, among which some of the more popular and widely used frameworks are listed below:

- TensorFlow (Python, C, Java, Go, JavaScript, Swift): <https://www.tensorflow.org/>
- Keras (Python): <https://keras.io/>
- PyTorch (Python, C++): <https://pytorch.org/>
- Caffe (Python, MATLAB): <http://caffe.berkeleyvision.org/>
- Chainer (Python): <https://chainer.org/>
- Deeplearning4j (Java, Scala, Python, Clojure, Kotlin): <https://deeplearning4j.org/>

- Microsoft Cognitive Toolkit (CNTK) (Python, C#, C++): <https://docs.microsoft.com/en-us/cognitive-toolkit/>
- Theano (Python): <http://www.deeplearning.net/software/theano/>
- MXNet (Python, Scala, Julia, R, Clojure, Java, C++, Perl): <https://mxnet.apache.org/>
- ONNX (Python): <https://microsoft.github.io/onnxruntime/>
- Sonnet (Python): <https://github.com/deepmind/sonnet>
- PaddlePaddle (Python): <https://github.com/PaddlePaddle/Paddle>
- DeepGraphLibrary (Python): <https://www.dgl.ai/>

### 7.2 SDKs

- NVIDIA CUDA-X AI platforms: <https://developer.nvidia.com/deep-learning-software>
- Qualcomm mobile platforms: <https://developer.qualcomm.com/solutions/artificial-intelligence>

### 7.3 Datasets

The following includes some popular benchmarking datasets and databases for medical image segmentation tasks:

- ISBI 2012 cell segmentation challenge: Electron microscopy cell slices. [http://brainiac2.mit.edu/isbi\\_challenge/](http://brainiac2.mit.edu/isbi_challenge/)

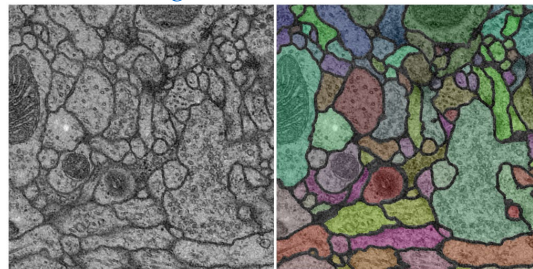


**Figure 12.** Example of ssTEM image and its corresponding segmentation from ISBI 2012 cell segmentation challenge [271].

- ISBI cell tracking challenge: Database collecting 2D and 3D time-lapse videos of moving cells from past and ongoing ISBI challenges. <http://celltrackingchallenge.net/>
- LiTS: Liver CT scans for tumor detection. <https://competitions.codalab.org/competitions/17094>
- LIDC-IDRI: Lung CT scans for cancer detection. <https://wiki.cancerimagingarchive.net/display/Public/LIDC-IDRI>
- DRIVE: A popular retinal fundus image dataset. <https://drive.grand-challenge.org/>

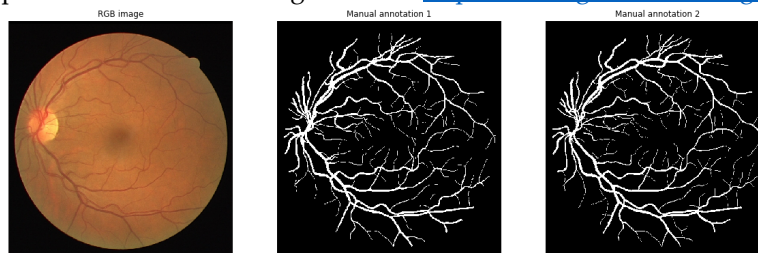


**Figure 13.** Fundus sample image along with corresponding ground truths from DRIVE [272].

- CT Colonography: CT scan dataset for colon cancer detection. <https://wiki.cancerimagingarchive.net/display/Public/CT+COLONOGRAPHY>
- Kaggle Data Science Bowl 2018: Nuclei segmentation challenge in microscopy images. <https://www.kaggle.com/c/data-science-bowl-2018>

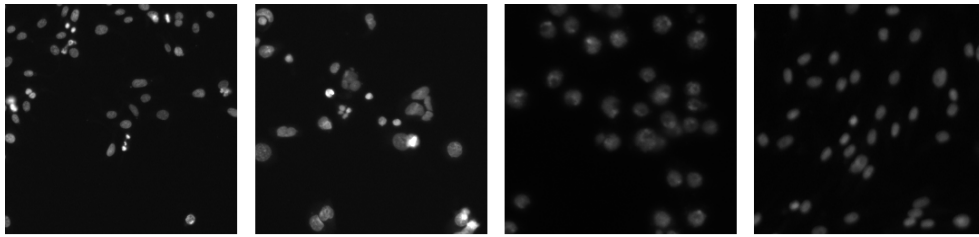


**Figure 14.** Example images from Kaggle data science bowl 2018 [273].

- ISIC archive: Database of Dermoscopy images from past and ongoing ISIC challenges. <https://www.isic-archive.com/>

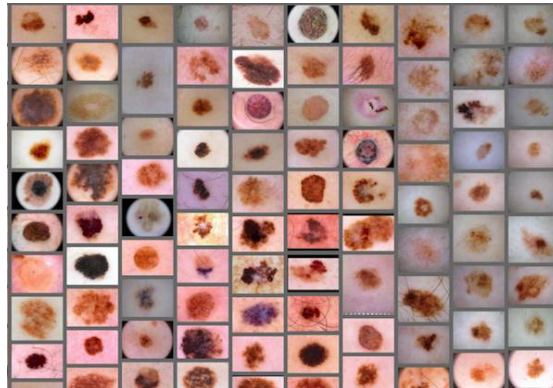


**Figure 15.** Examples of Dermoscopy images from the ISIC 2018 challenge [274], [275].

- SICAS Medical Image Repository: Archive for MICCAI Brain Tumor Segmentation Challenge (BRATS), MICCAI Ischemic Stroke Lesion Segmentation Challenge (ISLES), and ISBI Statistical Shape Model Challenge (SHAPE). <https://www.smir.ch/Home/Browse>

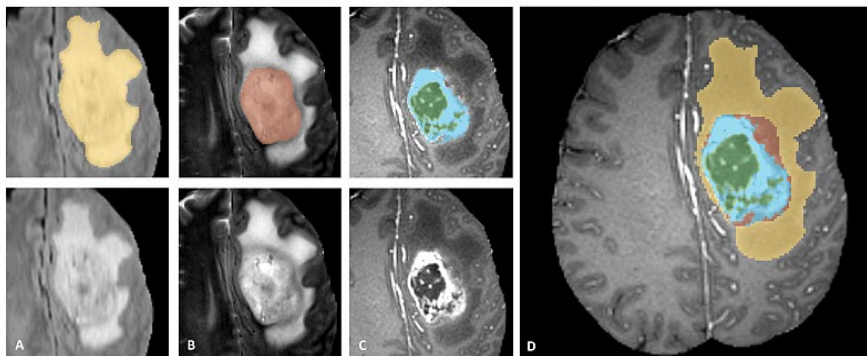


**Figure 16.** Example from Brain Tumor Segmentation Challenge (BRATS) 2017 [276]–[278].

- Medical Segmentation Decathlon: Collection of MR and CT databases for various target areas. <http://medicaldecathlon.com/>
- OASIS: Brain MRI and PET images. <https://www.oasis-brains.org/>
- ABIDE: Brain MRI datasets. [http://fcon\\_1000.projects.nitrc.org/indi/abide/](http://fcon_1000.projects.nitrc.org/indi/abide/)
- ICCVB: Prostate MRI and retinal fundus datasets. <http://i2cvb.github.io/>
- STARE: Retinal fundus dataset. <http://cecas.clemson.edu/~ahoover/stare/>

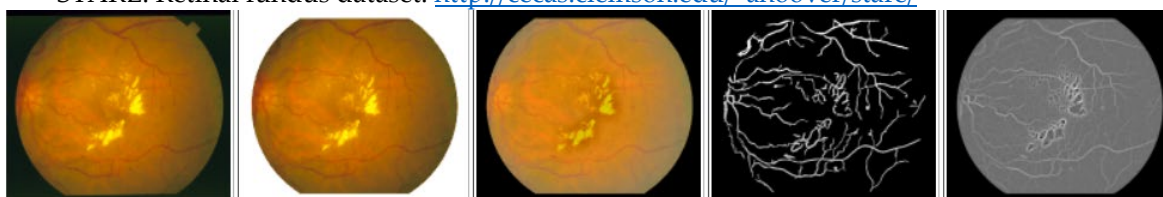


**Figure 17.** Example of STARE dataset showing the raw image, masked image, equalized image,

vessels, and MSF vessels [279], [280].

- CHASE\_DB1: Retinal fundus dataset. <https://blogs.kingston.ac.uk/retinal/chasedb1/>
- SCR: Chest X-ray dataset. <http://www.isi.uu.nl/Research/Databases/SCR/>

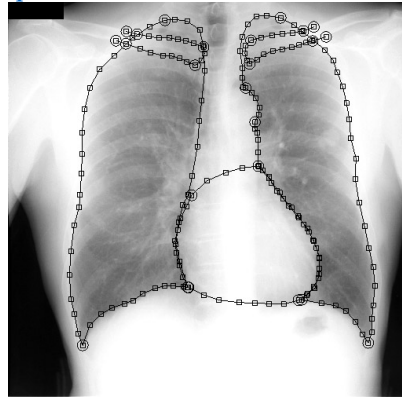


**Figure 18.** Example image from the SCR dataset. The lung field, the heart, and the clavicle are outlined [281], [282].

- DDSM: Mammogram dataset. <http://www.eng.usf.edu/cvprg/Mammography/Database.html>

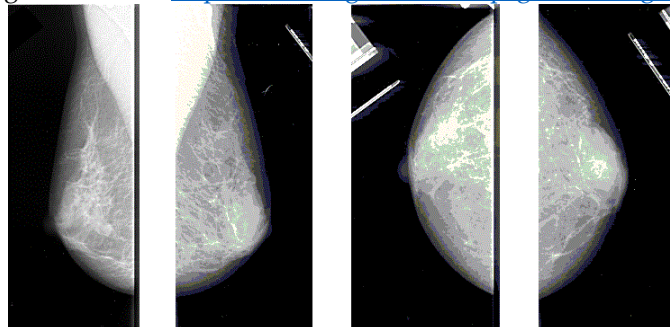


**Figure 19.** Sample images from the DDSM dataset [283], [284].

- BCDR: Mammogram database. <https://bcdr.eu/>
- mini-MIAS: Mammogram dataset. <http://peipa.essex.ac.uk/info/mias.html>
- PanNuke: Histology dataset for nuclei instance segmentation. <https://jgamper.github.io/PanNukeDataset/>

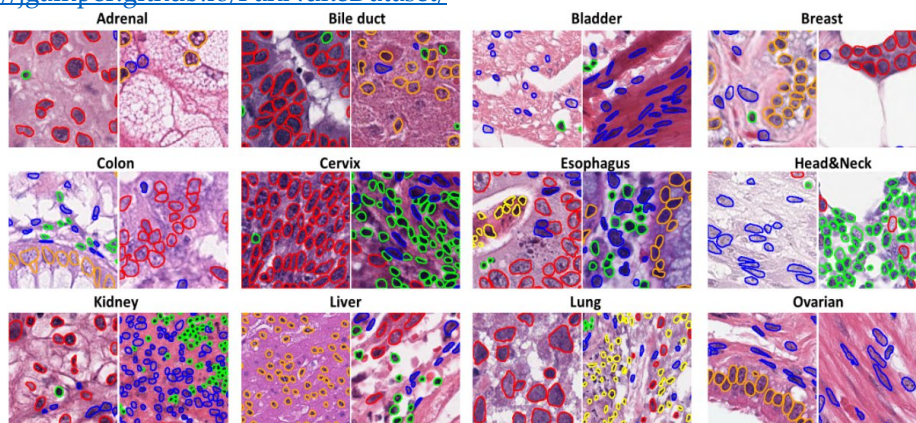


**Figure 20.** Ground truth of samples of different tissues from the PanNuke dataset [285], [286].

- University of Cyprus: Multiple sclerosis MRI, tele-orthopedics X-ray, and carotid ultrasound datasets. <http://www.ehealthlab.cs.ucy.ac.cy/index.php/facilities/32-software/218-datasets>
- The cancer imaging archive: A large public repository of cancer image datasets. <https://www.cancerimagingarchive.net/>

- Cardiac atlas project: Repository of cardiovascular image datasets. <http://www.cardiacatlas.org/>

#### 7.4 COVID-19 Datasets

The following are some publicly available COVID-19 image datasets.

- COVID-CT: <https://github.com/UCSD-AI4H/COVID-CT>
- COVID-19 CT: <http://medicalsegmentation.com/covid19/>
- University of Montreal COVID-19 Image Data Collection: <https://github.com/ieee8023/covid-chestxray-dataset>
- RadiologyAi Consortium: <https://www.radiologyaiconsortium.org/view>

#### 7.5 Conferences & Journals

Conferences:

- AAAI Conference on Artificial Intelligence (AAAI)
- British Machine Vision Conference (BMVC)
- Conference on Computer Vision and Pattern Recognition (CVPR)
- European Conference on Computer Vision (ECCV)
- International Conference on Computer Vision (ICCV)
- International Conference on Image Processing (ICIP)
- International Conference on Intelligent Robots and Systems (IROS)
- International Conference on Machine Learning (ICML)
- Medical Image Computing and Computer Assisted Intervention (MICCAI)
- Neural Information Processing Systems (NIPS)

Journals:

- IEEE Transactions on Image Processing
- IEEE Transactions on Medical Imaging
- IEEE Transactions on Pattern Analysis and Machine Intelligence
- International Journal of Computer Vision
- Journal of the American Medical Informatics Association
- Medical Image Analysis

#### References

- [1] O. Ronneberger, P. Fischer, and T. Brox, “U-net: Convolutional networks for biomedical image segmentation,” 2015, pp. 234–241.
- [2] J. Long, E. Shelhamer, and T. Darrell, “Fully convolutional networks for semantic segmentation,” 2015, pp. 3431–3440.
- [3] Ö. Çiçek, A. Abdulkadir, S. S. Lienkamp, T. Brox, and O. Ronneberger, “3D U-Net: learning dense volumetric segmentation from sparse annotation,” 2016, pp. 424–432.
- [4] Q. Tong, M. Ning, W. Si, X. Liao, and J. Qin, “3D deeply-supervised U-net based whole heart segmentation,” 2017, pp. 224–232.
- [5] C. Wang, T. MacGillivray, G. Macnaught, G. Yang, and D. Newby, “A Two-Stage U-Net Model for 3D Multi-class Segmentation on Full-Resolution Cardiac Data,” 2018, pp. 191–199.
- [6] S. Jia *et al.*, “Automatically segmenting the left atrium from cardiac images using successive 3D U-nets and a contour loss,” 2018, pp. 221–229.
- [7] S. R. Ravichandran *et al.*, “3D Inception U-Net for Aorta Segmentation using Computed Tomography Cardiac Angiography,” 2019, pp. 1–4.

- [8] H. Xu, Z. Xu, W. Gu, and Q. Zhang, "A Two-Stage Fully Automatic Segmentation Scheme Using Both 2D and 3D U-Net for Multi-sequence Cardiac MR," 2019, pp. 309–316.
- [9] T. Wang *et al.*, "MSU-Net: Multiscale Statistical U-Net for Real-time 3D Cardiac MRI Video Segmentation," 2019, pp. 614–622.
- [10] J. Wu, Y. Zhang, and X. Tang, "Simultaneous Tissue Classification and Lateral Ventricle Segmentation via a 2D U-net Driven by a 3D Fully Convolutional Neural Network," 2019, pp. 5928–5931.
- [11] D. Yang, Q. Huang, L. Axel, and D. Metaxas, "Multi-component deformable models coupled with 2D-3D U-Net for automated probabilistic segmentation of cardiac walls and blood," 2018, pp. 479–483.
- [12] G. Zeng, X. Yang, J. Li, L. Yu, P.-A. Heng, and G. Zheng, "3D U-net with multi-level deep supervision: fully automatic segmentation of proximal femur in 3D MR images," 2017, pp. 274–282.
- [13] G. Zeng *et al.*, "Latent3DU-net: Multi-level latent shape space constrained 3D U-net for automatic segmentation of the proximal femur from radial MRI of the hip," 2018, pp. 188–196.
- [14] G. Zeng and G. Zheng, "3D Tiled Convolution for Effective Segmentation of Volumetric Medical Images," 2019, pp. 146–154.
- [15] J. C. G. Sánchez, M. Magnusson, M. Sandborg, Å. C. Tedgren, and A. Malusek, "Segmentation of bones in medical dual-energy computed tomography volumes using the 3D U-Net," *Phys. Med.*, vol. 69, pp. 241–247, 2020.
- [16] H.-J. Bae *et al.*, "Fully automated 3D segmentation and separation of multiple cervical vertebrae in CT images using a 2D convolutional neural network," *Comput. Methods Programs Biomed.*, vol. 184, p. 105119, 2020.
- [17] C. Wang, Y. Guo, W. Chen, and Z. Yu, "Fully Automatic Intervertebral Disc Segmentation Using Multimodal 3D U-Net," 2019, vol. 1, pp. 730–739.
- [18] R. Mehta and T. Arbel, "3D U-Net for brain tumour segmentation," 2018, pp. 254–266.
- [19] W. Chen, B. Liu, S. Peng, J. Sun, and X. Qiao, "S3D-UNet: separable 3D U-Net for brain tumor segmentation," 2018, pp. 358–368.
- [20] M. Kolarik, R. Burget, V. Uher, and L. Povoda, "Superresolution of MRI brain images using unbalanced 3D Dense-U-Net network," 2019, pp. 643–646.
- [21] J. Owlser, B. Irving, G. Ridgeway, M. Wojciechowska, J. McGonigle, and M. Brady, "Comparison of Multi-atlas Segmentation and U-Net Approaches for Automated 3D Liver Delineation in MRI," 2019, pp. 478–488.
- [22] Q. Huang, J. Sun, H. Ding, X. Wang, and G. Wang, "Robust liver vessel extraction using 3D U-Net with variant dice loss function," *Comput. Biol. Med.*, vol. 101, pp. 153–162, 2018.
- [23] W. Yu, B. Fang, Y. Liu, M. Gao, S. Zheng, and Y. Wang, "Liver Vessels Segmentation Based on 3d Residual U-NET," 2019, pp. 250–254.
- [24] C. Zhao, J. Han, Y. Jia, and F. Gou, "Lung nodule detection via 3D U-Net and contextual convolutional neural network," 2018, pp. 356–361.

- [25] Y. He, X. Yu, C. Liu, J. Zhang, K. Hu, and H. C. Zhu, "A 3D Dual Path U-Net of Cancer Segmentation Based on MRI," 2018, pp. 268–272.
- [26] M. P. Heinrich, O. Oktay, and N. Bouteldja, "OBELISK-Net: Fewer layers to solve 3D multi-organ segmentation with sparse deformable convolutions," *Med. Image Anal.*, vol. 54, pp. 1–9, 2019.
- [27] H. Kakeya, T. Okada, and Y. Oshiro, "3D U-JAPA-Net: mixture of convolutional networks for abdominal multi-organ CT segmentation," 2018, pp. 426–433.
- [28] C. Huang, H. Han, Q. Yao, S. Zhu, and S. K. Zhou, "3D U<sup>2</sup>-Net: A 3D Universal U-Net for Multi-domain Medical Image Segmentation," 2019, pp. 291–299.
- [29] Y. Wang, L. Zhao, M. Wang, and Z. Song, "Organ at Risk Segmentation in Head and Neck CT Images Using a Two-Stage Segmentation Framework Based on 3D U-Net," *IEEE Access*, vol. 7, pp. 144591–144602, 2019.
- [30] B. Li, M. de Groot, M. W. Vernooij, M. A. Ikram, W. J. Niessen, and E. E. Bron, "Reproducible white matter tract segmentation using 3D U-Net on a large-scale DTI dataset," 2018, pp. 205–213.
- [31] O. Oktay *et al.*, "Attention u-net: Learning where to look for the pancreas," *ArXiv Prepr. ArXiv180403999*, 2018.
- [32] J. Schlemper *et al.*, "Attention gated networks: Learning to leverage salient regions in medical images," *Med. Image Anal.*, vol. 53, pp. 197–207, 2019.
- [33] A. Vaswani *et al.*, "Attention is all you need," 2017, pp. 5998–6008.
- [34] Z. Zhang, H. Fu, H. Dai, J. Shen, Y. Pang, and L. Shao, "ET-Net: A Generic Edge-attention Guidance Network for Medical Image Segmentation," 2019, pp. 442–450.
- [35] Z. Si, D. Fu, and J. Li, "U-Net with Attention Mechanism for Retinal Vessel Segmentation," in *Image and Graphics*, Cham, 2019, pp. 668–677.
- [36] L. Mou *et al.*, "CS-Net: Channel and Spatial Attention Network for Curvilinear Structure Segmentation," in *Medical Image Computing and Computer Assisted Intervention – MICCAI 2019*, Cham, 2019, pp. 721–730.
- [37] S. Lian, Z. Luo, Z. Zhong, X. Lin, S. Su, and S. Li, "Attention guided U-Net for accurate iris segmentation," *J. Vis. Commun. Image Represent.*, vol. 56, pp. 296–304, 2018.
- [38] C. Wu, Y. Zou, and Z. Yang, "U-GAN: Generative Adversarial Networks with U-Net for Retinal Vessel Segmentation," in *2019 14th International Conference on Computer Science & Education (ICCSE)*, Aug. 2019, pp. 642–646, doi: 10.1109/ICCSE.2019.8845397.
- [39] N. Abraham and N. M. Khan, "A novel focal tversky loss function with improved attention u-net for lesion segmentation," 2019, pp. 683–687.
- [40] H. Zhang, H. Zhu, and X. Ling, "Polar coordinate sampling-based segmentation of overlapping cervical cells using attention U-Net and random walk," *Neurocomputing*, vol. 383, pp. 212–223, 2020.
- [41] Z. Fang, Y. Chen, D. Nie, W. Lin, and D. Shen, "RCA-U-Net: Residual Channel Attention U-Net for Fast Tissue Quantification in Magnetic Resonance Fingerprinting," 2019, pp. 101–109.
- [42] C. Szegedy *et al.*, "Going deeper with convolutions," 2015, pp. 1–9.

- [43]C. Szegedy, V. Vanhoucke, S. Ioffe, J. Shlens, and Z. Wojna, “Rethinking the inception architecture for computer vision,” 2016, pp. 2818–2826.
- [44]H. Li, A. Li, and M. Wang, “A novel end-to-end brain tumor segmentation method using improved fully convolutional networks,” *Comput. Biol. Med.*, vol. 108, pp. 150–160, 2019.
- [45]Z. Zhang, C. Wu, S. Coleman, and D. Kerr, “DENSE-INception U-net for medical image segmentation,” *Comput. Methods Programs Biomed.*, vol. 192, p. 105395, 2020.
- [46]L. Chen, P. Bentley, K. Mori, K. Misawa, M. Fujiwara, and D. Rueckert, “DRINet for medical image segmentation,” *IEEE Trans. Med. Imaging*, vol. 37, no. 11, pp. 2453–2462, 2018.
- [47]A. H. Curiale, F. D. Colavecchia, and G. Mato, “Automatic quantification of the LV function and mass: a deep learning approach for cardiovascular MRI,” *Comput. Methods Programs Biomed.*, vol. 169, pp. 37–50, 2019.
- [48]H. Cheng, Y. Zhu, and H. Pan, “Modified U-Net block network for lung nodule detection,” 2019, pp. 599–605.
- [49]R. M. Rad, P. Saeedi, J. Au, and J. Havelock, “Trophectoderm segmentation in human embryo images via inceptioned U-Net,” *Med. Image Anal.*, vol. 62, p. 101612, 2020.
- [50]H. Zhao and N. Sun, “Improved U-Net Model for Nerve Segmentation,” in *Image and Graphics*, Cham, 2017, pp. 496–504.
- [51]K. He, X. Zhang, S. Ren, and J. Sun, “Deep residual learning for image recognition,” 2016, pp. 770–778.
- [52]M. Z. Alom, C. Yakopcic, T. M. Taha, and V. K. Asari, “Nuclei segmentation with recurrent residual convolutional neural networks based U-Net (R2U-Net),” 2018, pp. 228–233.
- [53]S. Das, A. Deka, Y. Iwahori, M. Bhuyan, T. Iwamoto, and J. Ueda, “Contour-Aware Residual W-Net for Nuclei Segmentation,” *Procedia Comput. Sci.*, vol. 159, pp. 1479–1488, 2019.
- [54]H. Li, A. Zhygallo, and B. Menze, “Automatic brain structures segmentation using deep residual dilated U-net,” 2018, pp. 385–393.
- [55]T. Mostafiz, I. Jarin, S. A. Fattah, and C. Shahnaz, “Retinal Blood Vessel Segmentation Using Residual Block Incorporated U-Net Architecture and Fuzzy Inference System,” in *2018 IEEE International WIE Conference on Electrical and Computer Engineering (WIECON-ECE)*, Dec. 2018, pp. 106–109, doi: 10.1109/WIECON-ECE.2018.8783182.
- [56]H. Li, D. Chen, W. H. Nilon, M. E. Davies, and D. Laurensen, “Improved breast mass segmentation in mammograms with conditional residual u-net,” in *Image Analysis for Moving Organ, Breast, and Thoracic Images*, Springer, 2018, pp. 81–89.
- [57]Y. Liu, N. Qi, Q. Zhu, and W. Li, “CR-U-Net: Cascaded U-Net with Residual Mapping for Liver Segmentation in CT Images,” 2019, pp. 1–4.
- [58]M. Baldeon-Calisto and S. K. Lai-Yuen, “AdaResU-Net: Multiobjective adaptive convolutional neural network for medical image segmentation,” *Neurocomputing*, 2019.
- [59]N. Ibtehaz and M. S. Rahman, “MultiResUNet: Rethinking the U-Net architecture for multimodal biomedical image segmentation,” *Neural Netw.*, vol. 121, pp. 74–87, 2020.

- [60]R. Zhang, L. Huang, W. Xia, B. Zhang, B. Qiu, and X. Gao, "Multiple supervised residual network for osteosarcoma segmentation in CT images," *Comput. Med. Imaging Graph.*, vol. 63, pp. 1–8, 2018.
- [61]K. Kawagoe, K. Hatano, S. Murakami, H. Lu, H. Kim, and T. Aoki, "Automatic Segmentation Method of Phalange Regions Based on Residual U-Net and MSGVF Snakes," in *2019 19th International Conference on Control, Automation and Systems (ICCAS)*, Oct. 2019, pp. 1046–1049, doi: 10.23919/ICCAS47443.2019.8971740.
- [62]E. Kerfoot, J. Clough, I. Oksuz, J. Lee, A. P. King, and J. A. Schnabel, "Left-ventricle quantification using residual u-net," 2018, pp. 371–380.
- [63]M. Liang and X. Hu, "Recurrent convolutional neural network for object recognition," 2015, pp. 3367–3375.
- [64]P. Q. Lee *et al.*, "Model-free prostate cancer segmentation from dynamic contrast-enhanced MRI with recurrent convolutional networks: A feasibility study," *Comput. Med. Imaging Graph.*, vol. 75, pp. 14–23, 2019.
- [65]B. Ji *et al.*, "A multi-scale recurrent fully convolution neural network for laryngeal leukoplakia segmentation," *Biomed. Signal Process. Control*, vol. 59, p. 101913, 2020.
- [66]M. Z. Alom, M. Hasan, C. Yakopcic, T. M. Taha, and V. K. Asari, "Recurrent residual convolutional neural network based on u-net (r2u-net) for medical image segmentation," *ArXiv Prepr. ArXiv180206955*, 2018.
- [67]G. Huang, Z. Liu, L. Van Der Maaten, and K. Q. Weinberger, "Densely connected convolutional networks," 2017, pp. 4700–4708.
- [68]C. Meng, K. Sun, S. Guan, Q. Wang, R. Zong, and L. Liu, "Multiscale dense convolutional neural network for DSA cerebrovascular segmentation," *Neurocomputing*, vol. 373, pp. 123–134, 2020.
- [69]J. Dolz, I. B. Ayed, and C. Desrosiers, "Dense multi-path U-Net for ischemic stroke lesion segmentation in multiple image modalities," 2018, pp. 271–282.
- [70]R. Azad, M. Asadi-Aghbolaghi, M. Fathy, and S. Escalera, "Bi-Directional ConvLSTM U-Net with Densely Connected Convolutions," 2019, pp. 0–0.
- [71]X. Li, H. Chen, X. Qi, Q. Dou, C.-W. Fu, and P.-A. Heng, "H-DenseUNet: hybrid densely connected UNet for liver and tumor segmentation from CT volumes," *IEEE Trans. Med. Imaging*, vol. 37, no. 12, pp. 2663–2674, 2018.
- [72]Z.-H. Wang, Z. Liu, Y.-Q. Song, and Y. Zhu, "Densely connected deep U-Net for abdominal multi-organ segmentation," 2019, pp. 1415–1419.
- [73]Z. Zhou, M. M. R. Siddiquee, N. Tajbakhsh, and J. Liang, "Unet++: A nested u-net architecture for medical image segmentation," in *Deep Learning in Medical Image Analysis and Multimodal Learning for Clinical Decision Support*, Springer, 2018, pp. 3–11.
- [74]J. Ren, H. Sun, Y. Huang, and H. Gao, "Knowledge-Based Multi-sequence MR Segmentation via Deep Learning with a Hybrid U-Net++ Model," 2019, pp. 280–289.
- [75]H. Cui, X. Liu, and N. Huang, "Pulmonary vessel segmentation based on orthogonal fused u-net++ of chest ct images," 2019, pp. 293–300.

- [76] S. Wu, Z. Wang, C. Liu, C. Zhu, S. Wu, and K. Xiao, "Automatic segmentation of pelvic organs after hysterectomy by using dilated convolution u-net++," 2019, pp. 362–367.
- [77] I. Goodfellow *et al.*, "Generative adversarial nets," 2014, pp. 2672–2680.
- [78] M. Mirza and S. Osindero, "Conditional generative adversarial nets," *ArXiv Prepr. ArXiv14111784*, 2014.
- [79] Y. Chen, A. Jakary, S. Avadiappan, C. P. Hess, and J. M. Lupo, "Qsmgan: Improved quantitative susceptibility mapping using 3d generative adversarial networks with increased receptive field," *NeuroImage*, vol. 207, p. 116389, 2020.
- [80] G. Yang *et al.*, "DAGAN: Deep de-aliasing generative adversarial networks for fast compressed sensing MRI reconstruction," *IEEE Trans. Med. Imaging*, vol. 37, no. 6, pp. 1310–1321, 2017.
- [81] Y. Xue, T. Xu, H. Zhang, L. R. Long, and X. Huang, "Segan: Adversarial network with multi-scale l1 loss for medical image segmentation," *Neuroinformatics*, vol. 16, no. 3–4, pp. 383–392, 2018.
- [82] T. Shen, C. Gou, F.-Y. Wang, Z. He, and W. Chen, "Learning from adversarial medical images for X-ray breast mass segmentation," *Comput. Methods Programs Biomed.*, vol. 180, p. 105012, Oct. 2019, doi: 10.1016/j.cmpb.2019.105012.
- [83] R. R. Upendra, S. Dangi, and C. A. Linte, "An Adversarial Network Architecture Using 2D U-Net Models for Segmentation of Left Ventricle from Cine Cardiac MRI," 2019, pp. 415–424.
- [84] G. Li, L. Zhang, S. Hu, D. Fu, and M. Liu, "Adversarial Network with Dual U-net Model and Multiresolution Loss Computation for Medical Images Registration," 2019, pp. 1–5.
- [85] X. Feng, C. Wang, S. Cheng, and L. Guo, "Automatic Liver and Tumor Segmentation of CT Based on Cascaded U-Net," 2019, pp. 155–164.
- [86] T. Liu, Y. Tian, S. Zhao, X. Huang, and Q. Wang, "Automatic Whole Heart Segmentation Using a Two-Stage U-Net Framework and an Adaptive Threshold Window," *IEEE Access*, vol. 7, pp. 83628–83636, 2019.
- [87] H. Liu, X. Shen, F. Shang, F. Ge, and F. Wang, "CU-Net: Cascaded U-Net with Loss Weighted Sampling for Brain Tumor Segmentation," in *Multimodal Brain Image Analysis and Mathematical Foundations of Computational Anatomy*, Springer, 2019, pp. 102–111.
- [88] X. Fu *et al.*, "M-Net: A Novel U-Net With Multi-Stream Feature Fusion and Multi-Scale Dilated Convolutions for Bile Ducts and Hepatolith Segmentation," *IEEE Access*, vol. 7, pp. 148645–148657, 2019.
- [89] J. Hong, B. Park, M. J. Lee, C.-S. Chung, J. Cha, and H. Park, "Two-step deep neural network for segmentation of deep white matter hyperintensities in migraineurs," *Comput. Methods Programs Biomed.*, vol. 183, p. 105065, 2020.
- [90] D. M. Vigneault, W. Xie, C. Y. Ho, D. A. Bluemke, and J. A. Noble, "Ω-net (omega-net): fully automatic, multi-view cardiac MR detection, orientation, and segmentation with deep neural networks," *Med. Image Anal.*, vol. 48, pp. 95–106, 2018.

- [91] J. Hu *et al.*, “S-UNet: A Bridge-Style U-Net Framework With a Saliency Mechanism for Retinal Vessel Segmentation,” *IEEE Access*, vol. 7, pp. 174167–174177, 2019, doi: 10.1109/ACCESS.2019.2940476.
- [92] M. K. Abd-Allah, A. A. Khalaf, A. I. Awad, and H. F. Hamed, “TPUAR-Net: Two Parallel U-Net with Asymmetric Residual-Based Deep Convolutional Neural Network for Brain Tumor Segmentation,” 2019, pp. 106–116.
- [93] M. Soltanpour, R. Greiner, P. Boulanger, and B. Buck, “Ischemic Stroke Lesion Prediction in CT Perfusion Scans Using Multiple Parallel U-Nets Following by a Pixel-Level Classifier,” 2019, pp. 957–963.
- [94] L. Zhang and L. Xu, “An Automatic Liver Segmentation Algorithm for CT Images U-Net with Separated Paths of Feature Extraction,” 2018, pp. 294–298.
- [95] D. Kwon *et al.*, “Siamese U-Net with Healthy Template for Accurate Segmentation of Intracranial Hemorrhage,” 2019, pp. 848–855.
- [96] M. Dunnhofer *et al.*, “Siam-U-Net: encoder-decoder siamese network for knee cartilage tracking in ultrasound images,” *Med. Image Anal.*, vol. 60, p. 101631, Feb. 2020, doi: 10.1016/j.media.2019.101631.
- [97] B. Murugesan, K. Sarveswaran, S. M. Shankaranarayana, K. Ram, J. Joseph, and M. Sivaprakasam, “Psi-Net: Shape and boundary aware joint multi-task deep network for medical image segmentation,” 2019, pp. 7223–7226.
- [98] K. Hu, C. Liu, X. Yu, J. Zhang, Y. He, and H. Zhu, “A 2.5 D Cancer Segmentation for MRI Images Based on U-Net,” 2018, pp. 6–10.
- [99] G. Piantadosi, M. Sansone, R. Fusco, and C. Sansone, “Multi-planar 3D breast segmentation in MRI via deep convolutional neural networks,” *Artif. Intell. Med.*, vol. 103, p. 101781, 2020.
- [100] C. Angermann and M. Haltmeier, “Random 2.5 D U-net for Fully 3D Segmentation,” in *Machine Learning and Medical Engineering for Cardiovascular Health and Intravascular Imaging and Computer Assisted Stenting*, Springer, 2019, pp. 158–166.
- [101] J. Wei, Y. Xia, and Y. Zhang, “M3Net: A multi-model, multi-size, and multi-view deep neural network for brain magnetic resonance image segmentation,” *Pattern Recognit.*, vol. 91, pp. 366–378, 2019.
- [102] Q. Jin, Z. Meng, T. D. Pham, Q. Chen, L. Wei, and R. Su, “DUNet: A deformable network for retinal vessel segmentation,” *Knowl.-Based Syst.*, vol. 178, pp. 149–162, Aug. 2019, doi: 10.1016/j.knosys.2019.04.025.
- [103] S. K. Hasan and C. A. Linte, “A Modified U-Net Convolutional Network Featuring a Nearest-neighbor Re-sampling-based Elastic-Transformation for Brain Tissue Characterization and Segmentation,” 2018, pp. 1–5.
- [104] L. Song, K. Geoffrey, and H. Kaijian, “Bottleneck feature supervised U-Net for pixel-wise liver and tumor segmentation,” *Expert Syst. Appl.*, vol. 145, p. 113131, 2020.
- [105] A. Colonna, F. Scarpa, and A. Ruggeri, “Segmentation of corneal nerves using a U-Net-based convolutional neural network,” in *Computational Pathology and Ophthalmic Medical Image Analysis*, Springer, 2018, pp. 185–192.

- [106] H. Dong, G. Yang, F. Liu, Y. Mo, and Y. Guo, "Automatic brain tumor detection and segmentation using u-net based fully convolutional networks," 2017, pp. 506–517.
- [107] H. T. Le and H. T.-T. Pham, "Brain Tumor Segmentation Using U-Net Based Deep Neural Networks," 2018, pp. 39–42.
- [108] A. Kerimi, I. Mahmoudi, and M. T. Khadir, "Deep convolutional neural networks using U-Net for automatic brain tumor segmentation in multimodal MRI volumes," 2018, pp. 37–48.
- [109] S. Chen, C. Ding, and M. Liu, "Dual-force convolutional neural networks for accurate brain tumor segmentation," *Pattern Recognit.*, vol. 88, pp. 90–100, 2019.
- [110] X. Kong, G. Sun, Q. Wu, J. Liu, and F. Lin, "Hybrid pyramid U-Net model for brain tumor segmentation," 2018, pp. 346–355.
- [111] A. Bousseham, O. Bouattane, M. Youssfi, and A. Raihani, "Improved Brain Tumor Segmentation in MRI Images Based on Thermal Analysis Model Using U-Net and GPUs," 2019, pp. 80–87.
- [112] Y. Chen, Z. Cao, C. Cao, J. Yang, and J. Zhang, "A modified U-net for brain MR image segmentation," 2018, pp. 233–242.
- [113] Z. Wu, F. Chen, and D. Wu, "A Novel Framework Called HDU for Segmentation of Brain Tumor," 2018, pp. 81–84.
- [114] T. Yang and J. Song, "An Automatic Brain Tumor Image Segmentation Method Based on the U-net," 2018, pp. 1600–1604.
- [115] J. Dutta, D. Chakraborty, and D. Mondal, "Multimodal Segmentation of Brain Tumours in Volumetric MRI Scans of the Brain Using Time-Distributed U-Net," in *Computational Intelligence in Pattern Recognition*, Springer, 2020, pp. 715–725.
- [116] R. Mehta, T. Christinck, T. Nair, P. Lemaitre, D. Arnold, and T. Arbel, "Propagating Uncertainty Across Cascaded Medical Imaging Tasks for Improved Deep Learning Inference," in *Uncertainty for Safe Utilization of Machine Learning in Medical Imaging and Clinical Image-Based Procedures*, Springer, 2019, pp. 23–32.
- [117] A. K. Dhara *et al.*, "Segmentation of post-operative glioblastoma in mri by u-net with patient-specific interactive refinement," 2018, pp. 115–122.
- [118] A. Rafi *et al.*, "U-Net Based Glioblastoma Segmentation with Patient's Overall Survival Prediction," 2020, pp. 22–32.
- [119] P. X. Nguyen, Z. Lu, W. Huang, S. Huang, A. Katsuki, and Z. Lin, "Medical Image Segmentation with Stochastic Aggregated Loss in a Unified U-Net," 2019, pp. 1–4.
- [120] Y. Xu, M. Gong, H. Fu, D. Tao, K. Zhang, and K. Batmanghelich, "Multi-scale masked 3-D U-net for brain tumor segmentation," 2018, pp. 222–233.
- [121] K. B. Dev, P. S. Jogi, S. Niyas, S. Vinayagamani, C. Kesavadas, and J. Rajan, "Automatic detection and localization of Focal Cortical Dysplasia lesions in MRI using fully convolutional neural network," *Biomed. Signal Process. Control*, vol. 52, pp. 218–225, 2019.
- [122] A. Zaman, L. Zhang, J. Yan, and D. Zhu, "Multi-modal Image Prediction via Spatial Hybrid U-Net," 2019, pp. 1–9.
- [123] M. Jafari *et al.*, "FU-Net: Multi-class Image Segmentation Using Feedback Weighted U-Net," 2019, pp. 529–537.

- [124] W. Yao, S. Wang, and H. Fu, "Hippocampus Segmentation in MRI Using Side U-Net Model," 2019, pp. 143–150.
- [125] Y. Zhang, W. Chen, Y. Chen, and X. Tang, "A post-processing method to improve the white matter hyperintensity segmentation accuracy for randomly-initialized U-net," 2018, pp. 1–5.
- [126] J. Wu, Y. Zhang, K. Wang, and X. Tang, "Skip Connection U-Net for White Matter Hyperintensities Segmentation From MRI," *IEEE Access*, vol. 7, pp. 155194–155202, 2019.
- [127] Y. Zhang *et al.*, "Fully Automatic White Matter Hyperintensity Segmentation using U-net and Skip Connection," 2019, pp. 974–977.
- [128] S. S. M. Salehi, D. Erdogmus, and A. Gholipour, "Auto-context convolutional neural network (auto-net) for brain extraction in magnetic resonance imaging," *IEEE Trans. Med. Imaging*, vol. 36, no. 11, pp. 2319–2330, 2017.
- [129] A. Rampun, D. Jarvis, P. Griffiths, and P. Armitage, "Automated 2D Fetal Brain Segmentation of MR Images Using a Deep U-Net," 2019, pp. 373–386.
- [130] J. Lou *et al.*, "Automatic Fetal Brain Extraction Using Multi-stage U-Net with Deep Supervision," 2019, pp. 592–600.
- [131] G. Wang *et al.*, "Interactive medical image segmentation using deep learning with image-specific fine tuning," *IEEE Trans. Med. Imaging*, vol. 37, no. 7, pp. 1562–1573, 2018.
- [132] G. R. Pinheiro, R. Voltoline, M. Bento, and L. Rittner, "V-Net and U-Net for Ischemic Stroke Lesion Segmentation in a Small Dataset of Perfusion Data," 2018, pp. 301–309.
- [133] R. Karthik, U. Gupta, A. Jha, R. Rajalakshmi, and R. Menaka, "A deep supervised approach for ischemic lesion segmentation from multimodal MRI using Fully Convolutional Network," *Appl. Soft Comput.*, vol. 84, p. 105685, 2019.
- [134] A. Bousseham, O. Bouattane, M. Youssfi, and A. Raihani, "Ischemic Stroke Lesion Segmentation Based on Thermal Analysis Model Using U-Net Fully Convolutional Neural Networks on GPUs," 2019, pp. 99–106.
- [135] L. K. S. Cornelio, M. A. V. del Castillo, and P. C. Naval Jr, "U-ISLES: Ischemic Stroke Lesion Segmentation Using U-Net," 2018, pp. 326–336.
- [136] J. Kobold *et al.*, "Stroke Thrombus Segmentation on SWAN with Multi-Directional U-Nets," 2019, pp. 1–6.
- [137] H. Yang, Z. Liu, and X. Yang, "Right Ventricle Segmentation in Short-Axis MRI Using a Shape Constrained Dense Connected U-Net," 2019, pp. 532–540.
- [138] Y.-C. Kim, K. R. Kim, and Y. H. Choe, "Automatic myocardial segmentation in dynamic contrast enhanced perfusion MRI using Monte Carlo dropout in an encoder-decoder convolutional neural network," *Comput. Methods Programs Biomed.*, vol. 185, p. 105150, 2020.
- [139] W. Yan, Y. Wang, Z. Li, R. J. Van Der Geest, and Q. Tao, "Left ventricle segmentation via optical-flow-net from short-axis cine MRI: preserving the temporal coherence of cardiac motion," 2018, pp. 613–621.

- [140] J. Zhang, J. Du, H. Liu, X. Hou, Y. Zhao, and M. Ding, "LU-NET: An improved U-Net for ventricular segmentation," *IEEE Access*, vol. 7, pp. 92539–92546, 2019.
- [141] S. Charmchi, K. Punithakumar, and P. Boulanger, "Optimizing U-net to segment left ventricle from magnetic resonance imaging," 2018, pp. 327–332.
- [142] G. Borodin and O. Senyukova, "Right ventricle segmentation in cardiac MR images using u-net with partly dilated convolution," 2018, pp. 179–185.
- [143] X. Wang *et al.*, "SK-Unet: an improved u-net model with selective kernel for the segmentation of multi-sequence cardiac MR," 2019, pp. 246–253.
- [144] X.-Y. Zhou, P. Li, Z.-Y. Wang, and G.-Z. Yang, "U-net training with instance-layer normalization," 2019, pp. 101–108.
- [145] W. Yan, Y. Wang, R. J. van der Geest, and Q. Tao, "Cine MRI analysis by deep learning of optical flow: Adding the temporal dimension," *Comput. Biol. Med.*, vol. 111, p. 103356, 2019.
- [146] F. Guo, M. Ng, and G. Wright, "Cardiac MRI Left Ventricle Segmentation and Quantification: A Framework Combining U-Net and Continuous Max-Flow," 2018, pp. 450–458.
- [147] R. J. Nowling *et al.*, "Classification before Segmentation: Improved U-Net Prostate Segmentation," 2019, pp. 1–4.
- [148] Y. Zhang, J. Wu, W. Chen, Y. Chen, and X. Tang, "Prostate segmentation using Z-net," 2019, pp. 11–14.
- [149] L. Rundo *et al.*, "USE-Net: Incorporating Squeeze-and-Excitation blocks into U-Net for prostate zonal segmentation of multi-institutional MRI datasets," *Neurocomputing*, vol. 365, pp. 31–43, 2019.
- [150] S. Elguindi *et al.*, "Deep learning-based auto-segmentation of targets and organs-at-risk for magnetic resonance imaging only planning of prostate radiotherapy," *Phys. Imaging Radiat. Oncol.*, vol. 12, pp. 80–86, 2019.
- [151] Y. Weng, T. Zhou, Y. Li, and X. Qiu, "NAS-Unet: Neural architecture search for medical image segmentation," *IEEE Access*, vol. 7, pp. 44247–44257, 2019.
- [152] A. Fabijańska *et al.*, "U-CatcHCC: An Accurate HCC Detector in Hepatic DCE-MRI Sequences Based on an U-Net Framework," 2018, pp. 319–328.
- [153] Y. Wang *et al.*, "A Two-Step Automated Quality Assessment for Liver MR Images Based on Convolutional Neural Network," *Eur. J. Radiol.*, p. 108822, 2020.
- [154] B. Zhao, J. Soraghan, G. Di Caterina, and D. Grose, "Segmentation of head and neck tumours using modified U-net," 2019, pp. 1–4.
- [155] G. Piantadosi, S. Marrone, A. Galli, M. Sansone, and C. Sansone, "DCE-MRI Breast Lesions Segmentation with a 3TP U-Net Deep Convolutional Neural Network," 2019, pp. 628–633.
- [156] M. AskariHemmat *et al.*, "U-Net Fixed-Point Quantization for Medical Image Segmentation," in *Large-Scale Annotation of Biomedical Data and Expert Label Synthesis and Hardware Aware Learning for Medical Imaging and Computer Assisted Intervention*, Springer, 2019, pp. 115–124.
- [157] F. Paugam *et al.*, "Open-source pipeline for multi-class segmentation of the spinal cord with deep learning," *Magn. Reson. Imaging*, vol. 64, pp. 21–27, 2019.

- [158] M. Han *et al.*, “Automatic Segmentation of Human Placenta Images With U-Net,” *IEEE Access*, vol. 7, pp. 180083–180092, 2019.
- [159] Y. Kurata *et al.*, “Automatic segmentation of the uterus on MRI using a convolutional neural network,” *Comput. Biol. Med.*, vol. 114, p. 103438, 2019.
- [160] K. Ryu, N.-Y. Shin, D.-H. Kim, and Y. Nam, “Synthesizing T1 weighted MPRAGE image from multi echo GRE images via deep neural network,” *Magn. Reson. Imaging*, vol. 64, pp. 13–20, 2019.
- [161] B. E. Dewey *et al.*, “DeepHarmony: A deep learning approach to contrast harmonization across scanner changes,” *Magn. Reson. Imaging*, vol. 64, pp. 160–170, 2019.
- [162] Z. Liu *et al.*, “Liver CT sequence segmentation based with improved U-Net and graph cut,” *Expert Syst. Appl.*, vol. 126, pp. 54–63, 2019.
- [163] B. Sakboonyara and P. Taeprasartsit, “U-Net and Mean-Shift Histogram for Efficient Liver Segmentation from CT Images,” 2019, pp. 51–56.
- [164] T.-Y. Su and Y.-H. Fang, “Automatic Liver and Spleen Segmentation with CT Images Using Multi-channel U-net Deep Learning Approach,” 2019, pp. 33–41.
- [165] B. A. Skourt, A. El Hassani, and A. Majda, “Lung CT image segmentation using deep neural networks,” *Procedia Comput. Sci.*, vol. 127, pp. 109–113, 2018.
- [166] W. Tan, Y. Liu, H. Liu, J. Yang, X. Yin, and Y. Zhang, “A Segmentation Method of Lung Parenchyma From Chest CT Images Based on Dual U-Net,” 2019, pp. 1649–1656.
- [167] H. Shaziya, K. Shyamala, and R. Zaheer, “Automatic Lung Segmentation on Thoracic CT Scans Using U-Net Convolutional Network,” 2018, pp. 0643–0647.
- [168] G. Tong, Y. Li, H. Chen, Q. Zhang, and H. Jiang, “Improved U-NET network for pulmonary nodules segmentation,” *Optik*, vol. 174, pp. 460–469, 2018.
- [169] Z. Gu *et al.*, “CE-Net: context encoder network for 2D medical image segmentation,” *IEEE Trans. Med. Imaging*, vol. 38, no. 10, pp. 2281–2292, 2019.
- [170] Z. Liu *et al.*, “Segmentation of organs-at-risk in cervical cancer CT images with a convolutional neural network,” *Phys. Med.*, vol. 69, pp. 184–191, 2020.
- [171] N. Yagi, M. Nii, and S. Kobashi, “Abdominal Organ Area Segmentation using U-Net for Cancer Radiotherapy Support,” 2019, pp. 1210–1214.
- [172] C. Wang, B. Connolly, P. F. de Oliveira Lopes, A. F. Frangi, and Ö. Smedby, “Pelvis segmentation using multi-pass U-Net and iterative shape estimation,” 2018, pp. 49–57.
- [173] A. Kumar *et al.*, “Segmentation of Lung Field in HRCT Images Using U-Net Based Fully Convolutional Networks,” 2018, pp. 84–93.
- [174] S. Hernández-Juárez *et al.*, “Semantic Segmentation of Lung Tissues in HRCT Images by Means of a U-Net Convolutional Network,” 2019, pp. 426–434.
- [175] A. Yang, X. Jin, and L. Li, “CT Images Recognition of Pulmonary Tuberculosis Based on Improved Faster RCNN and U-Net,” 2019, pp. 93–97.
- [176] Y. Man, Y. Huang, J. Feng, X. Li, and F. Wu, “Deep Q learning driven ct pancreas segmentation with geometry-aware u-net,” *IEEE Trans. Med. Imaging*, vol. 38, no. 8, pp. 1971–1980, 2019.

- [177] L. Wang, B. Wang, and Z. Xu, "Tumor Segmentation Based on Deeply Supervised Multi-Scale U-Net," 2019, pp. 746–749.
- [178] A. Manvel, K. Vladimir, T. Alexander, and U. Dmitry, "Radiologist-Level Stroke Classification on Non-contrast CT Scans with Deep U-Net," 2019, pp. 820–828.
- [179] D. Zhang, J. Wang, J. H. Noble, and B. M. Dawant, "HeadLocNet: Deep convolutional neural networks for accurate classification and multi-landmark localization of head CTs," *Med. Image Anal.*, vol. 61, p. 101659, 2020.
- [180] T. Song, F. Meng, A. Rodríguez-Patón, P. Li, P. Zheng, and X. Wang, "U-Next: A Novel Convolution Neural Network With an Aggregation U-Net Architecture for Gallstone Segmentation in CT Images," *IEEE Access*, vol. 7, pp. 166823–166832, 2019.
- [181] L. Bargsten, M. Wendebourg, and A. Schlaefler, "Data Representations for Segmentation of Vascular Structures Using Convolutional Neural Networks with U-Net Architecture," 2019, pp. 989–992.
- [182] L. Luo, D. Chen, and D. Xue, "Retinal blood vessels semantic segmentation method based on modified U-Net," in *2018 Chinese Control And Decision Conference (CCDC)*, Jun. 2018, pp. 1892–1895, doi: 10.1109/CCDC.2018.8407435.
- [183] J. Devda and R. Eswari, "Pathological Myopia Image Analysis Using Deep Learning," *2nd Int. Conf. Recent Trends Adv. Comput. ICRTAC -DISRUP - TIV Innov. 2019 Novemb. 11-12 2019*, vol. 165, pp. 239–244, Jan. 2019, doi: 10.1016/j.procs.2020.01.084.
- [184] X. Xu, T. Tan, and F. Xu, "An Improved U-Net Architecture for Simultaneous Arteriole and Venule Segmentation in Fundus Image," in *Medical Image Understanding and Analysis*, Cham, 2018, pp. 333–340.
- [185] W. Yijie, L. Shixuan, C. Guogang, C. Cong, L. Mengxue, and Z. Xinyu, "Improved U-net fundus image segmentation method," in *2019 International Conference on Intelligent Informatics and Biomedical Sciences (ICIIBMS)*, Nov. 2019, pp. 110–113, doi: 10.1109/ICIIBMS46890.2019.8991481.
- [186] Z. Yan, X. Han, C. Wang, Y. Qiu, Z. Xiong, and S. Cui, "Learning Mutually Local-Global U-Nets For High-Resolution Retinal Lesion Segmentation In Fundus Images," in *2019 IEEE 16th International Symposium on Biomedical Imaging (ISBI 2019)*, Apr. 2019, pp. 597–600, doi: 10.1109/ISBI.2019.8759579.
- [187] S. Kumawat and S. Raman, "Local Phase U-net for Fundus Image Segmentation," in *ICASSP 2019 - 2019 IEEE International Conference on Acoustics, Speech and Signal Processing (ICASSP)*, May 2019, pp. 1209–1213, doi: 10.1109/ICASSP.2019.8683390.
- [188] C. Guo, M. Szemenyei, Y. Pei, Y. Yi, and W. Zhou, "SD-Unet: A Structured Dropout U-Net for Retinal Vessel Segmentation," in *2019 IEEE 19th International Conference on Bioinformatics and Bioengineering (BIBE)*, Oct. 2019, pp. 439–444, doi: 10.1109/BIBE.2019.00085.
- [189] S. Zhang *et al.*, "Simultaneous Arteriole and Venule Segmentation of Dual-Modal Fundus Images Using a Multi-Task Cascade Network," *IEEE Access*, vol. 7, pp. 57561–57573, 2019, doi: 10.1109/ACCESS.2019.2914319.

- [190] J. Civit-Masot, F. Luna-Perejón, S. Vicente-Díaz, J. M. Rodríguez Corral, and A. Civit, "TPU Cloud-Based Generalized U-Net for Eye Fundus Image Segmentation," *IEEE Access*, vol. 7, pp. 142379–142387, 2019, doi: 10.1109/ACCESS.2019.2944692.
- [191] B. Wang, S. Qiu, and H. He, "Dual Encoding U-Net for Retinal Vessel Segmentation," in *Medical Image Computing and Computer Assisted Intervention – MICCAI 2019*, Cham, 2019, pp. 84–92.
- [192] P. Xiuqin, Q. Zhang, H. Zhang, and S. Li, "A Fundus Retinal Vessels Segmentation Scheme Based on the Improved Deep Learning U-Net Model," *IEEE Access*, vol. 7, pp. 122634–122643, 2019, doi: 10.1109/ACCESS.2019.2935138.
- [193] S. Yu, D. Xiao, S. Frost, and Y. Kanagasingam, "Robust optic disc and cup segmentation with deep learning for glaucoma detection," *Comput. Med. Imaging Graph.*, vol. 74, pp. 61–71, Jun. 2019, doi: 10.1016/j.compmedimag.2019.02.005.
- [194] R. Zhao, W. Chen, and G. Cao, "Edge-Boosted U-Net for 2D Medical Image Segmentation," *IEEE Access*, vol. 7, pp. 171214–171222, 2019.
- [195] Y. Wu *et al.*, "Vessel-Net: Retinal Vessel Segmentation Under Multi-path Supervision," in *Medical Image Computing and Computer Assisted Intervention – MICCAI 2019*, Cham, 2019, pp. 264–272.
- [196] K. Chen, G. Xu, J. Qian, and C.-X. Ren, "A Bypass-Based U-Net for Medical Image Segmentation," 2019, pp. 155–164.
- [197] E. B. Kablan, H. Dogan, M. E. Ercin, S. Ersoz, and M. Ekinici, "An ensemble of fine-tuned fully convolutional neural networks for pleural effusion cell nuclei segmentation," *Comput. Electr. Eng.*, vol. 81, p. 106533, 2020.
- [198] A. O. Vuola, S. U. Akram, and J. Kannala, "Mask-RCNN and U-net ensembled for nuclei segmentation," 2019, pp. 208–212.
- [199] J. Zhao *et al.*, "PGU-net+: Progressive Growing of U-net+ for Automated Cervical Nuclei Segmentation," 2019, pp. 51–58.
- [200] Y. Huang, H. Zhu, P. Wang, and D. Dong, "Segmentation of Overlapping Cervical Smear Cells Based on U-Net and Improved Level Set," 2019, pp. 3031–3035.
- [201] M. Zhang, X. Li, M. Xu, and Q. Li, "RBC semantic segmentation for sickle cell disease based on deformable U-Net," 2018, pp. 695–702.
- [202] R. M. Rad, P. Saeedi, J. Au, and J. Havelock, "Multi-resolutional ensemble of stacked dilated u-net for inner cell mass segmentation in human embryonic images," 2018, pp. 3518–3522.
- [203] H. M. Saleh, N. H. Saad, and N. A. M. Isa, "Overlapping Chromosome Segmentation using U-Net: Convolutional Networks with Test Time Augmentation," *Procedia Comput. Sci.*, vol. 159, pp. 524–533, 2019.
- [204] E. Altinsoy, C. Yilmaz, J. Wen, L. Wu, J. Yang, and Y. Zhu, "Raw G-Band Chromosome Image Segmentation Using U-Net Based Neural Network," 2019, pp. 117–126.
- [205] Y. M. Kassim, O. Glinskii, V. Glinsky, V. Huxley, G. Guidoboni, and K. Palaniappan, "Deep U-Net Regression and Hand-Crafted Feature Fusion for Accurate Blood Vessel Segmentation," 2019, pp. 1445–1449.

- [206] A. Ojeda-Pat, A. Martin-Gonzalez, and R. Soberanis-Mukul, "Convolutional Neural Network U-Net for Trypanosoma cruzi Segmentation," 2020, pp. 118–131.
- [207] G. Bueno, M. M. Fernandez-Carrobles, L. Gonzalez-Lopez, and O. Deniz, "Glomerulosclerosis identification in whole slide images using semantic segmentation," *Comput. Methods Programs Biomed.*, vol. 184, p. 105273, 2020.
- [208] X. Hu and H. Yang, "DRU-net: a novel U-net for biomedical image segmentation," *IET Image Process.*, vol. 14, no. 1, pp. 192–200, 2019.
- [209] M. Dash, N. D. Londhe, S. Ghosh, A. Semwal, and R. S. Sonawane, "PsLSNet: Automated psoriasis skin lesion segmentation using modified U-Net-based fully convolutional network," *Biomed. Signal Process. Control*, vol. 52, pp. 226–237, 2019.
- [210] S. N. Hasan, M. Gezer, R. A. Azeez, and S. Gülseçen, "Skin Lesion Segmentation by using Deep Learning Techniques," 2019, pp. 1–4.
- [211] Z. Al Nazi and T. A. Abir, "Automatic Skin Lesion Segmentation and Melanoma Detection: Transfer Learning Approach with U-Net and DCNN-SVM," 2020, pp. 371–381.
- [212] P. Tang *et al.*, "Efficient skin lesion segmentation using separable-Unet with stochastic weight averaging," *Comput. Methods Programs Biomed.*, vol. 178, pp. 289–301, 2019.
- [213] E. Z. Chen, X. Dong, X. Li, H. Jiang, R. Rong, and J. Wu, "Lesion attributes segmentation for melanoma detection with multi-task u-net," 2019, pp. 485–488.
- [214] G. Asaeikheybari, J. Green, X. Qian, H. Jiang, and M.-C. Huang, "Medical image learning from a few/few training samples: Melanoma segmentation study," *Smart Health*, vol. 14, p. 100088, 2019.
- [215] L. Liu, L. Mou, X. X. Zhu, and M. Mandal, "Skin Lesion Segmentation Based on Improved U-net," 2019, pp. 1–4.
- [216] M. A. Al-Masni, M. A. Al-antari, M.-T. Choi, S.-M. Han, and T.-S. Kim, "Skin lesion segmentation in dermoscopy images via deep full resolution convolutional networks," *Comput. Methods Programs Biomed.*, vol. 162, pp. 221–231, 2018.
- [217] B. S. Lin, K. Michael, S. Kalra, and H. R. Tizhoosh, "Skin lesion segmentation: U-nets versus clustering," 2017, pp. 1–7.
- [218] D. R. Ramani and S. S. Ranjani, "U-Net Based Segmentation and Multiple Feature Extraction of Dermoscopic Images for Efficient Diagnosis of Melanoma," in *Computer Aided Intervention and Diagnostics in Clinical and Medical Images*, Springer, 2019, pp. 81–101.
- [219] T. L. A. van den Heuvel, H. Petros, S. Santini, C. L. de Korte, and B. van Ginneken, "Automated Fetal Head Detection and Circumference Estimation from Free-Hand Ultrasound Sweeps Using Deep Learning in Resource-Limited Countries," *Ultrasound Med. Biol.*, vol. 45, no. 3, pp. 773–785, Mar. 2019, doi: 10.1016/j.ultrasmedbio.2018.09.015.
- [220] T. Włodarczyk *et al.*, "Estimation of Preterm Birth Markers with U-Net Segmentation Network," in *Smart Ultrasound Imaging and Perinatal, Preterm and Paediatric Image Analysis*, Cham, 2019, pp. 95–103.

- [221] B. Du *et al.*, “A novel transcranial ultrasound imaging method with diverging wave transmission and deep learning approach,” *Comput. Methods Programs Biomed.*, vol. 186, p. 105308, Apr. 2020, doi: 10.1016/j.cmpb.2019.105308.
- [222] Y. Wang, C. Wei, Z. Wang, Q. Lu, and C. Wang, “A More Streamlined U-net for Nerve Segmentation in Ultrasound Images,” in *2018 Chinese Automation Congress (CAC)*, Dec. 2018, pp. 101–104, doi: 10.1109/CAC.2018.8623052.
- [223] Q. Zhang, Z. Cui, X. Niu, S. Geng, and Y. Qiao, “Image Segmentation with Pyramid Dilated Convolution Based on ResNet and U-Net,” in *Neural Information Processing*, Cham, 2017, pp. 364–372.
- [224] N. Abraham, K. Illanko, N. Khan, and D. Androutsos, “Deep Learning for Semantic Segmentation of Brachial Plexus Nerves in Ultrasound Images Using U-Net and M-Net,” in *2019 3rd International Conference on Imaging, Signal Processing and Communication (ICISPC)*, Jul. 2019, pp. 85–89, doi: 10.1109/ICISPC.2019.8935668.
- [225] M. Amiri, R. Brooks, and H. Rivaz, “Fine Tuning U-Net for Ultrasound Image Segmentation: Which Layers?,” in *Domain Adaptation and Representation Transfer and Medical Image Learning with Less Labels and Imperfect Data*, Cham, 2019, pp. 235–242.
- [226] J. Yang, M. Faraji, and A. Basu, “Robust segmentation of arterial walls in intravascular ultrasound images using Dual Path U-Net,” *Ultrasonics*, vol. 96, pp. 24–33, Jul. 2019, doi: 10.1016/j.ultras.2019.03.014.
- [227] S. Moradi *et al.*, “MFP-Unet: A novel deep learning based approach for left ventricle segmentation in echocardiography,” *Phys. Med.*, vol. 67, pp. 58–69, 2019.
- [228] X. Li *et al.*, “Multi-Task Refined Boundary-Supervision U-Net (MRBSU-Net) for Gastrointestinal Stromal Tumor Segmentation in Endoscopic Ultrasound (EUS) Images,” *IEEE Access*, vol. 8, pp. 5805–5816, 2020, doi: 10.1109/ACCESS.2019.2963472.
- [229] J. Ding, Z. Huang, M. Shi, and C. Ning, “Automatic Thyroid Ultrasound Image Segmentation Based on U-shaped Network,” in *2019 12th International Congress on Image and Signal Processing, BioMedical Engineering and Informatics (CISP-BMEI)*, Oct. 2019, pp. 1–5, doi: 10.1109/CISP-BMEI48845.2019.8966062.
- [230] S. Marques *et al.*, “Segmentation of gynaecological ultrasound images using different U-Net based approaches,” in *2019 IEEE International Ultrasonics Symposium (IUS)*, Oct. 2019, pp. 1485–1488, doi: 10.1109/ULTSYM.2019.8925948.
- [231] K. HATANO, S. MURAKAMI, H. LU, J. K. TAN, H. KIM, and T. AOKI, “Detection of Phalange Region Based on U-Net,” in *2018 18th International Conference on Control, Automation and Systems (ICCAS)*, Oct. 2018, pp. 1338–1342.
- [232] W. Wu, J. Zhang, H. Xie, Y. Zhao, S. Zhang, and L. Gu, “Automatic detection of coronary artery stenosis by convolutional neural network with temporal constraint,” *Comput. Biol. Med.*, vol. 118, p. 103657, Mar. 2020, doi: 10.1016/j.compbiomed.2020.103657.
- [233] M. Gherardini, E. Mazomenos, A. Menciassi, and D. Stoyanov, “Catheter segmentation in X-ray fluoroscopy using synthetic data and transfer learning with light

- U-nets,” *Comput. Methods Programs Biomed.*, vol. 192, p. 105420, Aug. 2020, doi: 10.1016/j.cmpb.2020.105420.
- [234] L. Ding, K. Zhao, X. Zhang, X. Wang, and J. Zhang, “A Lightweight U-Net Architecture Multi-Scale Convolutional Network for Pediatric Hand Bone Segmentation in X-Ray Image,” *IEEE Access*, vol. 7, pp. 68436–68445, 2019, doi: 10.1109/ACCESS.2019.2918205.
- [235] M. Frid-Adar, A. Ben-Cohen, R. Amer, and H. Greenspan, “Improving the Segmentation of Anatomical Structures in Chest Radiographs Using U-Net with an ImageNet Pre-trained Encoder,” in *Image Analysis for Moving Organ, Breast, and Thoracic Images*, Cham, 2018, pp. 159–168.
- [236] Y. Shu, X. Wu, and W. Li, “LVC-Net: Medical Image Segmentation with Noisy Label Based on Local Visual Cues,” in *Medical Image Computing and Computer Assisted Intervention – MICCAI 2019*, Cham, 2019, pp. 558–566.
- [237] H. Toda *et al.*, “Shape Recovery of Polyp Using Blood Vessel Detection and Matching Estimation by U-Net,” 2019, pp. 450–453.
- [238] J. Leng, Y. Liu, T. Zhang, P. Quan, and Z. Cui, “Context-aware u-net for biomedical image segmentation,” 2018, pp. 2535–2538.
- [239] D. J. Matuszewski and I.-M. Sintorn, “Reducing the U-Net size for practical scenarios: Virus recognition in electron microscopy images,” *Comput. Methods Programs Biomed.*, vol. 178, pp. 31–39, 2019.
- [240] J. I. Orlando *et al.*, “U2-Net: A Bayesian U-Net Model With Epistemic Uncertainty Feedback For Photoreceptor Layer Segmentation In Pathological OCT Scans,” in *2019 IEEE 16th International Symposium on Biomedical Imaging (ISBI 2019)*, Apr. 2019, pp. 1441–1445, doi: 10.1109/ISBI.2019.8759581.
- [241] I. Z. Matovinovic, S. Loncaric, J. Lo, M. Heisler, and M. Sarunic, “Transfer Learning with U-Net type model for Automatic Segmentation of Three Retinal Layers In Optical Coherence Tomography Images,” in *2019 11th International Symposium on Image and Signal Processing and Analysis (ISPA)*, Sep. 2019, pp. 49–53, doi: 10.1109/ISPA.2019.8868639.
- [242] S. Liu, D. P. Shamonin, G. Zahnd, A. F. W. van der Steen, T. van Walsum, and G. van Soest, “Healthy Vessel Wall Detection Using U-Net in Optical Coherence Tomography,” in *Machine Learning and Medical Engineering for Cardiovascular Health and Intravascular Imaging and Computer Assisted Stenting*, Cham, 2019, pp. 184–192.
- [243] Z. Chen, D. Li, H. Shen, H. Mo, Z. Zeng, and H. Wei, “Automated segmentation of fluid regions in optical coherence tomography B-scan images of age-related macular degeneration,” *Opt. Laser Technol.*, vol. 122, p. 105830, Feb. 2020, doi: 10.1016/j.optlastec.2019.105830.
- [244] R. Asgari, S. Waldstein, F. Schlanitz, M. Baratsits, U. Schmidt-Erfurth, and H. Bogunović, “U-Net with Spatial Pyramid Pooling for Drusen Segmentation in Optical Coherence Tomography,” in *Ophthalmic Medical Image Analysis*, Cham, 2019, pp. 77–85.

- [245] M. Zhang *et al.*, “A neural network approach to segment brain blood vessels in digital subtraction angiography,” *Comput. Methods Programs Biomed.*, vol. 185, p. 105159, 2020.
- [246] Y. Han and J. C. Ye, “Framing U-Net via deep convolutional framelets: Application to sparse-view CT,” *IEEE Trans. Med. Imaging*, vol. 37, no. 6, pp. 1418–1429, 2018.
- [247] Y. Liu *et al.*, “Artifact Suppression for Passive Cavitation Imaging Using U-Net CNNs with Uncertainty Quantification,” in *2019 IEEE 4th International Conference on Signal and Image Processing (ICSIP)*, Jul. 2019, pp. 1037–1042, doi: 10.1109/SIPROCESS.2019.8868593.
- [248] Z. Cheng, K. Guo, C. Wu, J. Shen, and L. Qu, “U-Net cascaded with dilated convolution for medical image registration,” 2019, pp. 3647–3651.
- [249] M. Salem *et al.*, “A fully convolutional neural network for new T2-w lesion detection in multiple sclerosis,” *NeuroImage Clin.*, vol. 25, p. 102149, 2020.
- [250] L. Sun *et al.*, “Topological correction of infant cortical surfaces using anatomically constrained U-net,” 2018, pp. 125–133.
- [251] I. Olaciregui-Ruiz, I. Torres-Xirau, J. Teuwen, U. A. van der Heide, and A. Mans, “A Deep Learning-based correction to EPID dosimetry for attenuation and scatter in the Unity MR-Linac system,” *Phys. Med.*, vol. 71, pp. 124–131, 2020.
- [252] G. Li, L. Bai, C. Zhu, E. Wu, and R. Ma, “A Novel Method of Synthetic CT Generation from MR Images Based on Convolutional Neural Networks,” 2018, pp. 1–5.
- [253] O. Lucena, R. Souza, L. Rittner, R. Frayne, and R. Lotufo, “Convolutional neural networks for skull-stripping in brain MR imaging using silver standard masks,” *Artif. Intell. Med.*, vol. 98, pp. 48–58, 2019.
- [254] G. Litjens *et al.*, “A survey on deep learning in medical image analysis,” *Med. Image Anal.*, vol. 42, pp. 60–88, 2017.
- [255] M. Bakator and D. Radosav, “Deep learning and medical diagnosis: A review of literature,” *Multimodal Technol. Interact.*, vol. 2, no. 3, p. 47, 2018.
- [256] S. Minaee, Y. Boykov, F. Porikli, A. Plaza, N. Kehtarnavaz, and D. Terzopoulos, “Image Segmentation Using Deep Learning: A Survey,” *ArXiv200105566 Cs*, Apr. 2020, Accessed: Jun. 08, 2020. [Online]. Available: <http://arxiv.org/abs/2001.05566>.
- [257] M. Tan and Q. V. Le, “Efficientnet: Rethinking model scaling for convolutional neural networks,” *ArXiv Prepr. ArXiv190511946*, 2019.
- [258] X. Yi, E. Walia, and P. Babyn, “Generative adversarial network in medical imaging: A review,” *Med. Image Anal.*, vol. 58, p. 101552, 2019.
- [259] N. Papernot, P. McDaniel, I. Goodfellow, S. Jha, Z. B. Celik, and A. Swami, “Practical black-box attacks against machine learning,” 2017, pp. 506–519.
- [260] M. I. Razzak, S. Naz, and A. Zaib, “Deep learning for medical image processing: Overview, challenges and the future,” in *Classification in BioApps*, Springer, 2018, pp. 323–350.
- [261] World Health Organization, “Coronavirus disease (COVID-2019) situation report 153.”  
[https://www.who.int/docs/default-source/coronaviruse/situation-reports/20200621-covid-19-sitrep-153.pdf?sfvrsn=c896464d\\_2](https://www.who.int/docs/default-source/coronaviruse/situation-reports/20200621-covid-19-sitrep-153.pdf?sfvrsn=c896464d_2) (accessed Jun. 22, 2020).

- [262] S. Jin *et al.*, “AI-assisted CT imaging analysis for COVID-19 screening: Building and deploying a medical AI system in four weeks,” *medRxiv*, 2020.
- [263] X. Chen, L. Yao, and Y. Zhang, “Residual Attention U-Net for Automated Multi-Class Segmentation of COVID-19 Chest CT Images,” *ArXiv Prepr. ArXiv200405645*, 2020.
- [264] T. Zhou, S. Canu, and S. Ruan, “An automatic COVID-19 CT segmentation based on U-Net with attention mechanism,” *ArXiv Prepr. ArXiv200406673*, 2020.
- [265] Y.-H. Wu *et al.*, “JCS: An explainable COVID-19 diagnosis system by joint classification and segmentation,” *ArXiv Prepr. ArXiv200407054*, 2020.
- [266] Q. Yan *et al.*, “COVID-19 Chest CT Image Segmentation--A Deep Convolutional Neural Network Solution,” *ArXiv Prepr. ArXiv200410987*, 2020.
- [267] G. Gaál, B. Maga, and A. Lukács, “Attention u-net based adversarial architectures for chest x-ray lung segmentation,” *ArXiv Prepr. ArXiv200310304*, 2020.
- [268] T. Ozturk, M. Talo, E. A. Yildirim, U. B. Baloglu, O. Yildirim, and U. R. Acharya, “Automated detection of COVID-19 cases using deep neural networks with X-ray images,” *Comput. Biol. Med.*, p. 103792, 2020.
- [269] M. Z. Alom, M. Rahman, M. S. Nasrin, T. M. Taha, and V. K. Asari, “COVID\_MNet: COVID-19 Detection with Multi-Task Deep Learning Approaches,” *ArXiv Prepr. ArXiv200403747*, 2020.
- [270] F. Shi *et al.*, “Review of artificial intelligence techniques in imaging data acquisition, segmentation and diagnosis for covid-19,” *IEEE Rev. Biomed. Eng.*, 2020.
- [271] I. Arganda-Carreras *et al.*, “Crowdsourcing the creation of image segmentation algorithms for connectomics,” *Front. Neuroanat.*, vol. 9, p. 142, 2015.
- [272] M. Niemeijer, J. Staal, B. Ginneken, M. Loog, and M. Abramoff, “DRIVE: digital retinal images for vessel extraction,” *Methods Eval. Segmentation Index. Tech. Dedic. Retin. Ophthalmol.*, 2004.
- [273] J. C. Caicedo *et al.*, “Nucleus segmentation across imaging experiments: the 2018 Data Science Bowl,” *Nat. Methods*, vol. 16, no. 12, pp. 1247–1253, 2019.
- [274] N. Codella *et al.*, “Skin lesion analysis toward melanoma detection 2018: A challenge hosted by the international skin imaging collaboration (isic),” *ArXiv Prepr. ArXiv190203368*, 2019.
- [275] P. Tschandl, C. Rosendahl, and H. Kittler, “The HAM10000 dataset, a large collection of multi-source dermatoscopic images of common pigmented skin lesions,” *Sci. Data*, vol. 5, p. 180161, 2018.
- [276] B. H. Menze *et al.*, “The multimodal brain tumor image segmentation benchmark (BRATS),” *IEEE Trans. Med. Imaging*, vol. 34, no. 10, pp. 1993–2024, 2014.
- [277] S. Bakas *et al.*, “Advancing the cancer genome atlas glioma MRI collections with expert segmentation labels and radiomic features,” *Sci. Data*, vol. 4, p. 170117, 2017.
- [278] S. Bakas *et al.*, “Identifying the best machine learning algorithms for brain tumor segmentation, progression assessment, and overall survival prediction in the BRATS challenge,” *ArXiv Prepr. ArXiv181102629*, 2018.

- [279] A. Hoover, V. Kouznetsova, and M. Goldbaum, "Locating blood vessels in retinal images by piecewise threshold probing of a matched filter response," *IEEE Trans. Med. Imaging*, vol. 19, no. 3, pp. 203–210, 2000.
- [280] A. Hoover and M. Goldbaum, "Locating the optic nerve in a retinal image using the fuzzy convergence of the blood vessels," *IEEE Trans. Med. Imaging*, vol. 22, no. 8, pp. 951–958, 2003.
- [281] B. Van Ginneken, M. B. Stegmann, and M. Loog, "Segmentation of anatomical structures in chest radiographs using supervised methods: a comparative study on a public database," *Med. Image Anal.*, vol. 10, no. 1, pp. 19–40, 2006.
- [282] J. Shiraishi *et al.*, "Development of a digital image database for chest radiographs with and without a lung nodule: receiver operating characteristic analysis of radiologists' detection of pulmonary nodules," *Am. J. Roentgenol.*, vol. 174, no. 1, pp. 71–74, 2000.
- [283] K. Bowyer *et al.*, "The digital database for screening mammography," 1996, vol. 58, p. 27.
- [284] M. Heath *et al.*, "Current status of the digital database for screening mammography," in *Digital mammography*, Springer, 1998, pp. 457–460.
- [285] J. Gamper, N. A. Koohbanani, K. Benet, A. Khuram, and N. Rajpoot, "PanNuke: an open pan-cancer histology dataset for nuclei instance segmentation and classification," 2019, pp. 11–19.
- [286] J. Gamper *et al.*, "PanNuke Dataset Extension, Insights and Baselines," *ArXiv Prepr. ArXiv200310778*, 2020.